University of Texas at El Paso
ScholarWorks@UTEP

Open Access Theses & Dissertations

2022-12-01

Exploring The Effect Of Environmental Degradation On The Shape Memory Properties Of Polymers

Jorge Mario Avila
University of Texas at El Paso

Follow this and additional works at: https://scholarworks.utep.edu/open_etd

 Part of the Polymer and Organic Materials Commons

Recommended Citation

Avila, Jorge Mario, "Exploring The Effect Of Environmental Degradation On The Shape Memory Properties Of Polymers" (2022). *Open Access Theses & Dissertations*. 3647.
https://scholarworks.utep.edu/open_etd/3647

This is brought to you for free and open access by ScholarWorks@UTEP. It has been accepted for inclusion in Open Access Theses & Dissertations by an authorized administrator of ScholarWorks@UTEP. For more information, please contact lweber@utep.edu.

EXPLORING THE EFFECT OF ENVIRONMENTAL DEGRADATION ON THE SHAPE MEMORY PROPERTIES OF POLYMERS

JORGE MARIO AVILA BARRAZA

Master's Program in Metallurgical & Materials Engineering

APPROVED:

David A. Roberson, Ph.D., Chair

Darren M. Cone, M.S.

Robert C. Roberts, Ph.D.

Stephen L. Crites, Jr., Ph.D.
Dean of the Graduate School

Copyright ©

by

Jorge Mario Avila Barraza

2022

DEDICATION

"This entire effort is in dedication to the memory of my father, the love of my mother, the support of my brother and the rest of my family and close friends that had been wishing me the best since the beginning until the end of my studies"

EXPLORING THE EFFECT OF ENVIRONMENTAL DEGRADATION ON THE SHAPE MEMORY PROPERTIES OF POLYMERS

by

JORGE MARIO AVILA BARRAZA, B.S.

THESIS

Presented to the Faculty of the Graduate School of

The University of Texas at El Paso

in Partial Fulfillment

of the Requirements

for the Degree of

MASTER OF SCIENCE

Department of Metallurgical, Materials and Biomedical Engineering

THE UNIVERSITY OF TEXAS AT EL PASO

December 2022

ACKNOWLEDGEMENTS

The completion of this study could not have been possible without the expertise of Dr. David A. Roberson, my thesis advisor, the facilities of the Polymer Extrusion Lab, and the support of my colleagues Truman J. Word & Brittany L. Payan. I would also like to thank M.Sc. Darren Cone & Dr. Roberts for sitting on our panel and taking the time to read my thesis.

A debt of gratitude is also owed to Mr. Lopez Reyes, former instructor of the electronics division at ITESM Campus Juarez, for pointing me toward the Metallurgy & Engineering Materials sections and providing me with the guides for my framework.

Last but not least, I would like to thank my parents – Mr. (dec.) and Mrs. Avila, without you none of this would indeed be possible. And a special thank you for my Güera, for pulling my ears when needed and supporting me along the way.

ABSTRACT

A key detriment of the use of polymers by our society is the negative effect this material class has had on the environment. A category of polymers known as shape memory polymers (SMP)s have the ability to return to a programmed original shape form after deformation to a temporary shape by using stimuli such as temperature, electrical pulses and even magnetism. The shape memory effect allows for some polymers to heal if they are damaged. This ability to heal means that components made from these materials can be reused rather than thrown away if they are damaged. The work presented in the thesis is intended to provide information related to the ability of a material to maintain shape memory properties and how these self-healing mechanisms can mitigate environmental degradation. Here, we compare the effects of two manufacturing techniques: additive manufacturing and injection molding in order to determine the influence of processing on material properties.

This effort is pursued based on the premise that self-healing materials provide an avenue for the reduction of polymeric waste, a problem that is growing more detrimental to the environment. The shape memory effect is a critical component of the self-healing process in polymers. It is my goal to contribute to the solvency of a societal problem by understanding the structure, process, property, performance relationship of novel shape memory polymeric systems.

TABLE OF CONTENTS

LIST OF TABLES

LIST OF FIGURES

CHAPTER 1: INTRODUCTION AND BACKGROUND

Plastic materials began to be produced on a large scale in the 1950s, for the manufacture of everyday products. It was a time when technology underwent a dramatic evolution and when humanity had blind faith in it, hoping that it would solve all the problems at the time, like liberating society from the social and economic constraints imposed by the scarcity of non-renewable natural resources and the rise of cost in metals due to increasing demand. (Gongora, 2014). Among other important events, in that decade were the invention of several items including the first microchip, the color television, the modem, the credit card. The polio vaccine was also used for the first time. Technological advances held the promise of furthering the advancement of humanity. At the same time, plastic began to takeover markets, product by product, and due to its practicality, durability, and convenience, it was replacing steel in cars, paper and glass in packaging, wool and cotton in clothing, and wood in furniture (Wicks, 2007). Starting in the 1970s, the first environmental movements were born, generating awareness for the first time about the environmental costs of economic progress (Sul & Costa, 2007). The reputation of plastic also declined in the 1970s and 1980s as concerns about waste and the notion that plastic does not biodegrade grew (Monteiro, Sul, & F.Costa, 2018). However, the petrochemical industry introduced the concept of recycling and left our consciences clear. We all surely remember the "3Rs: reduce, reuse and recycle". So, plastic continued among us adding uses, since, under a certain general assumption, or assumed by the majority, all plastic is recycled (Sakai, et al., 2011). Thus, plastic is still considered a wonder material and its use has continued to grow. Only now are we slowly beginning to realize and understand the problems that come with it.

The first and main problem, from which all the problems of plastic waste originate, is that nearly all plastics used by humankind are not biodegradable. And by biodegrading we mean that

there are no organisms that transform it into organic matter (Narayan, 2017). But make no mistake: the fact that plastic is not biodegradable does not mean that components made from plastic will remain intact for ever and ever. Plastic fragments, mechanically degrade and disintegrate and therefore remain in the environment as particles get smaller and smaller (Sharma & Chatterjee, 2017). The action of temperature, ultraviolet rays, wind, etc. break polymer parts down mechanically until what was once a relatively large piece of plastic is transformed into micro and nano plastic particles (Hamidian, et al., 2021). Second, plastic is not inert. In the manufacture polymermeric materials, several additives and chemical compounds are added to make plastics more flexible, durable, and transparent (Turner & Filella, 2021). These additives are not fully incorporated into the plastic matrix, so they can be released into the environment, and as the plastic breaks down and degrades, more additives are released, especially at high temperatures. For example, it has been reported that when a plastic container of water is heated to 40°C, some of its additives are transferred to the water (Hermabessiere, et al., 2017). Another example, a study conducted by the National Institutes of Health (NIH) showed that in 93% of people tested, the urine contained bisphenol A. In very high doses, these chemicals could disrupt the endocrine system (Kristen, et al., 2014). For this reason, this Institute recommends not heating food in plastic containers in the microwave, and avoiding canned foods because they contain bisphenol A. Both bisphenol A and phthalates (water bottles are made of polyethylene terephthalate, PET) accumulate and can affect the reproduction and development of animals, at concentrations that can be found in the environment (Ema, et al., 2001). Bisphenol A is also banned for use in baby bottles and pacifiers, and many manufacturers have stopped using it on their own, although alternative analogues have very similar toxicity (Aschberger, Castello, Hoekstra, Karakitsios, & S. Munn, 2010). Other additives commonly used in the production of plastics are flame retardants. Animal

and human toxicology studies have shown that some of these additives are potentially carcinogenic, toxic to neurons, and affect the human endocrine system (Chen, et al., 2014). Third, plastics can adsorb and accumulate other toxic compounds and pollutants from the environment. In addition, there is evidence that aquatic organisms accumulate chemical compounds after ingesting plastic (Guzzetti, Sureda, SilviaTejada, & Faggio, 2018).

Plastic garbage is generally divided into two categories: macro and micro plastics. The macro plastics have a length greater than 5mm and constitute the large fragments of plastic waste, such as remains of bags, fishing nets, bottles, bottle caps, etc. Microplastic is, by definition, less than 5mm in length, although it can be on the order of micrometers (thousandths of a millimeter) and nanometers (millionths of a millimeter) and is formed as large fragments that disintegrate by the mechanical action of wind, water, UV rays, etc., (Suaria, et al., 2020). In 1980 it was discovered that there are convergence zones in the sea, called "gyres", where garbage accumulates, due to flow of material which occurs as a result of winds and sea currents. These areas used to be called “plastic islands”, however, they are now better known as “plastic soups”, since microplastics were found to be the most abundant type of waste in water samples (Eriksen, et al., 2013). The five major ocean trash gyres that are currently found around the globe are illustrated in Fig 1.1 (Slat, 2022). Some estimates suggest that plastic makes up between 60% and 80% of marine debris. A recent study determined that the sea surface in the North Pacific gyre contains more plastic than naturally occurring floating debris and is dominated primarily by polyethylene and polypropylene (Egger, Sulu-Gambari, & Lebreton, 2020). We now know that the problem is global, as more accumulation zones have been found in various parts of the ocean, and large amounts of plastic have even been found in Arctic water samples (Bergmann, et al., 2022). Adverse physical impacts to organisms from macro plastics in aquatic environments, including ingestion, entanglement, and

suffocation, have been well documented, for example in work published by the Wageningen Institute for Marine Research in the Netherlands (Kühn, et al., 2018) which showed that plastic ingestion is less visible than entanglement but can lead to direct or indirect mortality due to poor nutrition or dehydration.

Figure 1.1 Ocean trash gyres current map

(Slat, 2022).

Recent scientific work has shown that more than half of the world's seabirds have ingested plastic, and that many species of fish also ingest plastic (KosukeTanaka, et al., 2013). The impact of microplastics is more difficult to assess because they do not cause direct mortality in most of the organisms that ingest them (Horn, Granek, & Steele, 2019). However, the plastic additives and the presence of other contaminants adsorbed on the surface of plastic particles could increase the toxicity. Since microplastics are hydrophobic (i.e., insoluble in water) and have a high surface area to volume ratio, they can absorb these contaminants and then pass them on to other organisms (Ziccardi, Edgington, Hentz, Kulacki, & Driscoll, 2016).

For now, there is no information about how plastic particles and their additives interact once ingested by animals. Since the microplastic particles are so small, they are impossible to remove from the environment, meaning that they are consumed by animals and microorganisms

(Smith, Love, Rochman, & Neff, 2018). Thus, microplastic enters the food chain since animals do not see it or consume it thinking it is food. This leads to bioaccumulation, since not all the plastic material that is eaten can be eliminated from the body. Without knowing it, humans are also consuming plastics (Cox, et al., 2019). Microplastics have recently been found in drinking water, in bottled water, in samples of salt for human consumption, in beer, honey, rainwater, in the deepest part of the sea, and in the Arctic (Welle & Franz, 2018). Also, as if this were not enough, microplastics were found in human feces (Schwabl, et al., 2019). Since the evidence confirms our daily exposure to microplastic, more studies are needed to determine the ability of plastics to bioaccumulate, adsorb and desorb pollutants (Akhbarizadeh, Moore, & Keshavarzi, 2019), to better understand the role of plastic within ecosystems and its risk to human health.

But what if plastics can endure more? What if plastics materials could have a longer life cycle lessening the frequency at which plastic parts are thrown away? This might be possible, but first, an understanding of how to mitigate damage incurred by harsh environmental conditions must be made. Plastic production can be modified by using the proper polymers to create this new generation of plastics and help reduce plastic waste, this is where shape memory polymers can join the cause (Lendlein & Kelch, 2002). The next paragraph includes an explanation of the basic principles of shape memory polymers, which is needed in order to understand the relation between SMP's and self-healing properties.

The shape memory effect represents the capability of shape memory materials to "memorize" their original shape and allow them to recover this original shape from a temporary deformed shape under appropriate stimuli. Shape memory effect involves two features: fixability and recoverability. Fixability refers to the capability of the shape memory materials to change from the original undeformed shape to a temporary deformed shape through a suitable programming

process (i.e., shape fixing). Recoverability indicates its ability to recover the original shape. Rf and Rr are calculated as follows:

$$Rf(\%) = \frac{\varepsilon u}{\varepsilon m}\ x\ 100\% \qquad (1)$$

$$Rr(\%) = \frac{\varepsilon m - \varepsilon p}{\varepsilon m} x\ 100\% \qquad (2)$$

Where deformation is performed in a tensile testing machine and εu is the elongation of the specimen after the load is removed, εm is the maximum strain the specimen is subjected to (usually100% elongation) and εp is the elongation of the specimen after recovery. In most cases involving thermoplastic shape memory polymers, recovery is achieved by heating the specimens.

In the programming process, shape memory materials are deformed mechanically, and the deformed shape fixed temporarily (Andreas Lendlein O. E., 2019). The most important characteristic of shape memory effect is the stability of this temporarily deformed shape, which does not change in the absence of suitable stimuli. The temporary shape is triggered actively to recover the original permanent shape by exposure to an appropriate stimulus. In general, heat, light, and electricity can be used for triggering. There are reports on SMP's triggered from other stimuli, such as magnetic-induced and water-driven effects. Among those effects, thermally induced are more common, and in which shape recovery takes place with respect to a certain critical temperature.

The shape memory effect (SME) of SMP's is not a specific property of a single polymer. It results from the structure and morphology of the polymer and is influenced by the programmed testing conditions. The prerequisite to achieve a SME involves two aspects, a net point (hard segment) and the switch (soft segment) (Mohadeseh Zare, 2019). The net point provides entropic elasticity and is responsible for shape recovery. The switch is reversibly sensitive to certain external stimuli and responsible for shape fixing. In general, in the permanent shape, the internal

stress is zero or very low. If the SMP is subjected to deformation, the internal stress can be "stored" in the polymer structure by following a suitable programming process. By exposing the polymer to a suitable stimulus, the shape memory polymer recovers its permanent shape as a result of releasing the internal stress stored in the crosslinking structure.

As an example, a thermally induced SMP. The elastic networks (hard segments) in the SMP can be created by chemical/physical crosslinking, as well as interpenetrating or any other approaches. The hard segments in the polymer network play the part of network conjunctions that can stabilize the network all along in the series of thermomechanical processes. The polymeric network chains have the role of 'switching domains' whose thermal transition temperature (Tt_{rans}) essentially serves as the T_{trans} for triggering SME. The molecular mobility of switching domains changes greatly above and below the T_{trans}, and the modulus of materials can thus change by ≥1–2 orders of magnitude in a narrow temperature range around the T_{trans}. The network chain segments are flexible at temperatures above the T_{trans} but rigid at temperatures below the T_{trans}, where the mobility of the chains is frozen (or at least limited). The polymer materials, therefore, can develop large deformations at temperatures above the T_{trans} and afterwards can fix into a temporary shape at temperatures below the T_{trans}. Fig. 1.2 illustrates the molecular mechanism of SME in a thermally induced SMP. According to the mechanism, the reversible phase, having a melting transition temperature of the soft segments as the Ttrans is used to hold the temporary deformation. The fixed phase is referred to the hard segments, which are linked to the soft segments via physical crosslinks. Hence, the fixed phase inhibits the plastic slip of the molecular chains by physical cross-linkage points among them and can be responsible for memorizing the permanent shape (Andreas Lendlein M. B., 2010).

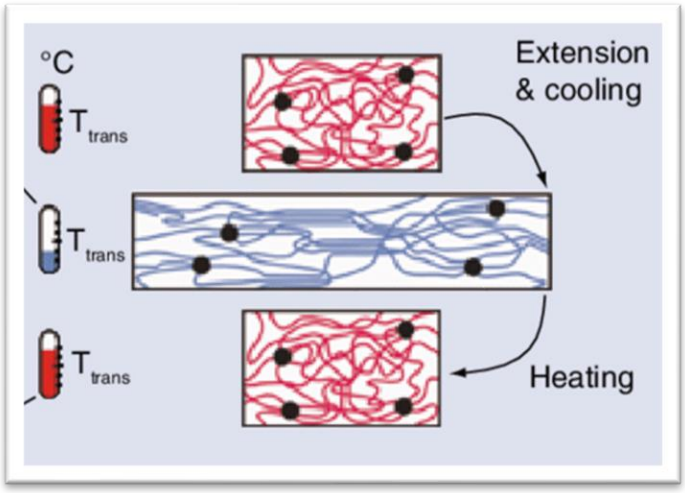

Figure 1.2 Schematic of the molecular mechanism of a thermally induced SMP

(Andreas Lendlein M. B., 2010).

However, SMP should have polymeric networks to effectively memorize their original shape. The major difference between 'traditional' polymeric elastomers and SMP lies in the different Ttrans of their polymeric network chains. Nevertheless, the SMP that can hold a temporary shape around room temperature will be more useful for practical applications. Therefore, the Ttrans of SMP is most often above room temperature. It can be concluded that SMP represent only a small section of the 'polymer family' and demonstrate SME under ambient conditions (Li Sun, 2010).

So, now with a clear understanding on the basic's fundamentals of SMPs, it can be inferred that these materials can be considered active, "smart" or even multifunctional; capable of responding in a reversible and controllable way by different external physical or chemical stimuli, by modifying some of its properties (Garces & Ayranci, 2021). Due to their sensitivity or performance, these materials can be used for the design and development of sensors, actuators, and multifunctional systems (Pilate, Toncheva, Dubois, & Raquez, 2016). Some of these materials have been known for many years and others (most) are of recent appearance. They are presented

in different natures: inorganic, metallic and organic, being sensitive to a wide variety of physical and chemical phenomena (Liu, Ding, Cao, Zheng, & Peng, 2005). Currently the importance of SMPs is driven by new needs in technologies such as microelectronics and nanoelectronics, as well as the possibility of developing structures, materials and products with predefined active properties and combined functions (Zarek, et al., 2015) .

Among the advantages of SMP's integrating multiple functions in a system, the size reductions of assemblies stand out, associated, the increase in the size of production series and the reduction of costs in materials and processes are economic factors that drives SMP's for further research. (Lantada, 2017). Active materials can play a decisive role in multiple future applications, since in themselves they relate electrical, thermal, chemical, optical, magnetic, and mechanical magnitudes (Lei, Chen, Lu, & Yu, 2019). The possible combined use of different families of active materials greatly enhances the industrial applications (aeronautics, architecture, communications, electronics, computing, medicine, robotics, and transport fundamentally).

Shape memory polymers have properties analogous to alloys with shape memory, since they present a mechanical response to changes in temperature (Hager, Bode, ChristineWeber, & Schubert, 2015). These polymers usually belong to families such as epoxy resins, polyurethane resins, polystyrenes, and styrene acrylates (Kumar, Biju, & Nair, 2013).

As a reminder, SMP's are materials that exhibit mechanical response against temperature, electrical and many other physical changes (Shi, Yoonessi, & Weiss, 2013). By heating these materials above their temperature of "activation", a radical change from rigid polymer to an elastic state is obtained, which allows deformations of up to 300% (Yakacki, S. Willis, & Gall, 2008). Once handled, if the material is cooled while maintaining the imposed deformation, said structure "freezes" returning to a rigid but "non-equilibrium" state (Westbrook, Kao, Castro, Ding, & Qi,

2011). By reheating the material above its activation temperature, the initial shape is recovered. not deformed. Fig. 1.3 demonstrates how a shape memory polymer can change their structure based on different transition stimulus (Pavia, 2022).

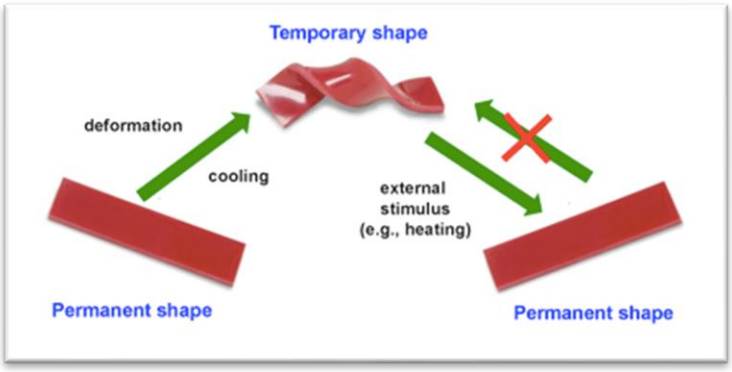

Figure 1.3 Example of a shape memory polymer transition

(Pavia, 2022).

The cycle can be repeated numerous times without degradation of the polymer and most suppliers can formulate different materials with activation temperatures between –30 ºC and 260 ºC, depending on the desired application (Xia, He, Zhang, Liu, & Leng, 2020). They are therefore active materials that present coupling thermomechanical and a high deformation recovery capacity, (much greater than that presented by shape memory alloys), which together with its lower density and cost has enhanced the design of numerous applications (Qi, Nguyen, Castro, Yakacki, & Shandas, 2008). The properties of SMPs allow applications in the manufacture of sensor devices - actuators, especially for the aeronautical, automotive, and medical fields (Sokolowski, Metcalfe, Hayashi, Yahia, & Raymond, Medical applications of shape memory polymers, 2007).

The use of SMPs as a substitute or complement for shape memory metal alloys is giving rise to numerous developments, which take advantage of thermomechanical coupling to obtain systems of detection – action (Liu, Gall, Dunn, & McCluskey, 2003). Numerous applications are

also being developed in medical devices, that take advantage of their properties by using them as actuators.

However, the relatively recent development and implementation of SMPs means that, in many cases, it's the mechanical and thermomechanical properties of these materials are not fully characterized, which increases uncertainty about the response of devices made from these materials (P.Butaud, et al., 2015). One of the fundamental objectives of the work performed here is to increase knowledge about the properties of these polymers, especially related to self-healing properties.

Self-healing polymers have the ability to transform physical energy into a chemical and/or physical response to heal the damage. Self-healing polymers response to external stimulus to recover the initial material properties. This condition can also be related with shape memory effects. In synthetic polymers, the shape-memory effect was discovered in the 1940's and first used in dental materials (methacrylic ester resin) (US Patent No. 2234993, 1941). In the 1960's, this discovery was followed by the development of heat-shrinkable polyethylene in films, tubing, and other applications (US Patent No. 3144398, 1964). The response of shape-memory materials to external stimuli was largely neglected as part of self-healing processes. Nevertheless, if designed properly, polymers can "memorize" a permanent shape that can be manipulated to create a temporary form, and, under suitable conditions triggered by external or internal stimuli (for example, heat, light, or deformation), transform back to the memorized permanent shape. Such responses manifest in conformational changes and/or chain contractions, which are typically entropy-driven, resulting in mass flow and self-healing (Cussler, 2009).

Incorporating soft and hard segments into one copolymer can lead to phase-separated morphologies. For example, a material that combines rubber elasticity and thermoplastic stiffness

will expand the applications of copolymers owing to enhanced mechanical properties represented by enhanced storage and loss moduli. If stiff and tough polymers are combined with dynamic and flexible macromolecular assemblies facilitating mobility, self-healing can be achieved (Mohr, 2006). The action of the shape-memory effect during self-healing restores entropic energy upon the release of the force creating damage to fill an open wound in the material.

Substantiated on this, the current research tries to mitigate environmental degradation with the help of self-healing mechanisms based on shape memory effect polymers. It is intended to study specific materials that can be submitted to certain conditions to observe their resistance and behavior and how can they possibly help reduce massive plastic production in order to avoid pollution and improve the manufacturing quality of all existent products.

CHAPTER 2: OBJECTIVES, SCIENCE QUESTIONS, AND TASKS

The main objective of this research is to discover how harsh environmental conditions affect shape memory performance of a polymer. Mechanical and chemical properties were valuated before and after environmental exposure. At the same time the shape memory properties were assessed for exposed and non-exposed specimens. The ultimate objective is to generate meaningful data about the behavior of these polymers under specific environmental conditions and determine the strengths and weaknesses of these materials.

For this work, we chose to use a shape memory polymer system that was developed to be compatible with the additive manufacturing (AM) platform of fused filament fabrication (FFF). The details of this system will be further discussed in this thesis. The shape memory properties of this material are already known, thus making this material system a good candidate for assessing the effect of environmental conditions on shape memory properties. The material was composed of a combination of polylactic acid (PLA) and styrene ethylene butylene styrene (SEBS) that was first melt compounded and extruded in the form of a filament that is compatible with FFF printers. Some of the material was then pelletized for use in plastic injection molding. By utilizing two manufacturing methods we will also be able to understand the relationship between processing technique and degradation mechanisms.

Another important aspect was to determine if shape memory polymers could mitigate, as self healing mechanisms, any environmental degradation (TaoXu, GuoqiangLi, & Pang, 2011). By looking directly at the effect of environmental degradation on shape memory properties we sought to answer this second research objective. The key enabler in meeting this research objective was the methodology implemented for the grouping experimentation. A point of comparison between

regular condition affected samples is the best scenario to verify the behavior of these materials under different environmental situations (humidity & temperature).

The last objective consisted of making a manufacturing process characterization (Dizon, Jr., Chen, & Advincula, 2018) to determine if 3D printed or injection molded specimens are more or less suceptible to environmental degradation based on the sample fabrication process.

2.1 Research Tasks

Task 1 – Filament Extrusion: This step involved the extrusion of a shape memory polymer blend by melt compounding two different polymers (PLA and SEBS) in a twin screw extruder that resulted in a well-blended filament. This filament was used to fabricate 30 tensile specimens using a FFF printer under the specifications of the ASTM Type IV standard using longitudinal raster pattern. Figure 2.1 illustrates the raster pattern, that was used for the printing of these specimens (Chávez, et al., 2019).

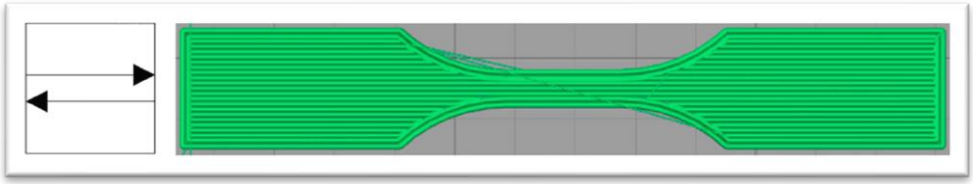

Figure 2.1 Schematic of the g-code filling pattern used: longitudinal, 0°

(Chávez, et al., 2019).

The remainder of the filament was pelletized and used to produce at least 6 specimens by the plastic injection mold process for comparison. These samples were segregated into multiple groups and tested under different circumstances.

Q1. Can environmental degradation be mitigated by heat-induced self-healing mechanisms?

Objective 1. Maintain a longer lifetime cycle of plastics by extruding a certain shape memory polymer blend that can help mitigate harsh environmental conditions.

Task 2 – Segregation of Samples & Testing: By making use of the grouped samples, the experimentation and methodology was divided by baseline and moisture exposure groups. This is needed in order to have a comparison point between: 1. Specimens that were not exposed to an environmental condition with no environmental factors added (effectively a control group) & 2. Plastics exposed to humidity as a primary environmental factor (the experimental group). All samples were submitted to a final tensile test for data recovery and summary. This will result in a full study determining any change in mechanical or chemical properties. Another test also evaluated the effect of moisture exposure on the shape memory properties. Further details will be discussed in the next chapter of this thesis.

Q2. What physical or chemical changes are induced by exposure to harsh environments?

Objective 2: Determine the different behaviors that harsh environmental conditions can create on mechanical or chemical properties of the samples.

Task 3 – Specimen Manufacturing Method Analysis: Once the entire experimentation has finished, the mechanical and chemical properties of both manufacturing processes (3D printing and plastic injection molding) (Komal, Kasaudhan, & Singh, 2021) were set for comparison analysis in order to determine which process is more prone to environmental degradation.

Q3. Are printed specimens susceptible to environmental degradation?

Objective 3: Obtain information from multiple testing regarding mechanical and chemical reactions between different specimens (3D printed & mold plastic injected) and compare the different aspects to determine the strengths and deficiencies.

Figure 2.2 illustrates a diagram based on the previous science questions and tasks formulated, this has been done to follow a proper method to achieve a final result regarding the objectives considered.

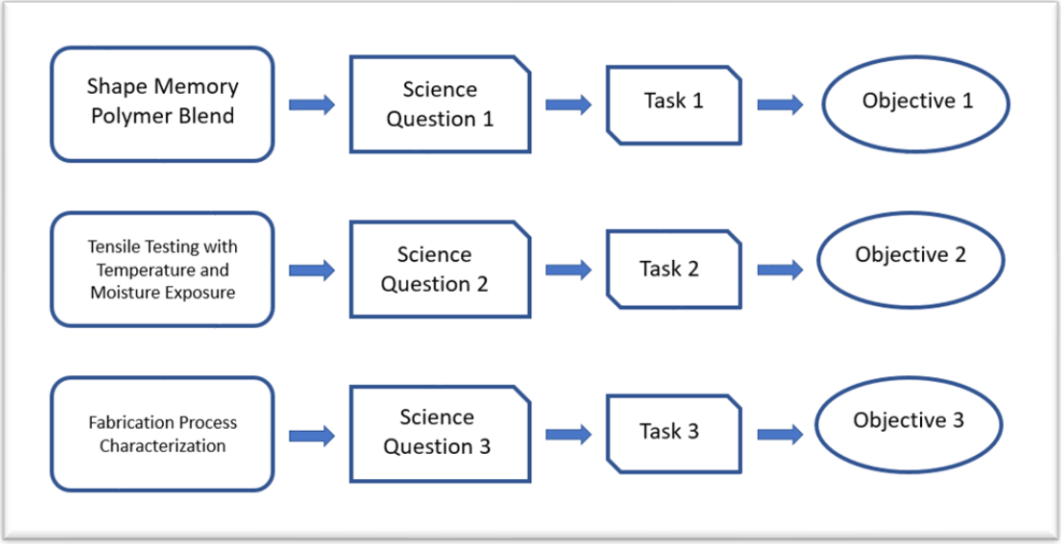

Figure 2.2 Science questions' diagram.

CHAPTER 3: EXPERIMENTAL PROCEDURE

The polymer blend used was a PLA 4043D – SEBS-g-MA (Ingeo Biopolymer Grade 4043D, NatureWorks, Minnetonka, MN, USA) in a 50/50 percent mix. This particular blend was purposely designed to be a shape memory polymer system in a previous effort conducted by the Polymer Extrusion Lab (Paulina A. Quinonez, 2021). Though PLA is rigid on its own, the combination of PLA with SEBS yields a ductile blend that can be deformed at room temperature. Both PLA and SEBS possess shape memory properties on their own (Paulina A. Quinonez, 2021). Before extruding, the polymers (in pellet form) were subjected to a drying process in order to remove any humidity within the material. For this batch, 400 g. (200 g. of PLA 4043D and 200 g. of SEB) were used. Materials were dried on a compressed air dryer as shown in Figure 3.1 (Micro Dryer CAFM station, Dri-Air Industries, East Windsor, CT, USA). PLA 4043D was dried for 2 hours at a temperature of 50°C and SEBS was dried overnight at a temperature of 80°C.

Figure 3.1 Micro Dryer CAFM (drying material equipment).

After drying, the constituents were melt compounded through the use of a polymer extruder. The equipment used for this extrusion was a twin screw extruder compounder (Model ZK-25T, Collin Lab and Pilot Solutions, Norcross, GA, USA). Before extruding the blend

material, the extruder was cleaned. The cleaning process consisted of manual brushing and cleaning of the internal screw and barrel components. Dyna Purge (thermoplastic purging compound) was also used to detach remains of materials that were extruded earlier, this material was also found in pellets. Dyna Purge (Grade D2, Schuman Plastics, Buffalo, NY, USA) was also used to detach remains of materials that were extruded earlier. Dyna Purge is also found in pellets form and is a proprietary mixture of polyethylene and detergents. First the Dyna Purge was poured in a small portion into the hopper, allowed to run through the system, and then the entire mix of the polymer blend was added. Our process was timed with the intent that, after 10 min, the Dyna Purge had been fully expunged from the extruder meaning that the blend was expected to come out pure as it needs to be without Dyna Purge (color difference is a visual aid). After this, the extruded mixture was manually drawn over an air cooler (Filabot Air Path, Filabot, Bare, VT, USA). The belt puller, component on the filament winder. The extruder system is seen in Figure 3.2. The belt puller was used to draw the filament to a target diameter of 1.85mm. Diameter of the filament was monitored manually by taking diameter measurements with a caliper. Diameter was controlled by modulating the speed of the belt puller. This is largely a manual process as there is no measurement system for the speed of the belt puller or filament winder. Extrusion parameters for the material used in this study can be found in Table 3-1:

Table 3-1 Extrusion Parameters.

Extrusion Parameters	
Zone 1	180
Zone 2	185
Zone 3	185
Zone 4	185
Zone 5	180
Zone 6	180
Pressure 1	90
Extruder Screws	16
Melt Pump Screws	12
Feed rate	10

Figure 3.2 Techline ZK 25 Compounder, cooler & belt puller with filament winder stations.

The process of extrusion was done twice to ensure total blending of the components. After the first extrusion, the filament as pelletized using a Collin pelletizer (Pelletizer CDG 171/1, Collin Lab and Pilot Solutions, Norcross, GA, USA) and extruded again. This time without the necessity of cleaning or running Dyna Purge through the machine. Both processes can be observed in Figure 3.3. After the second extrusion was done, the final filament was ready as shown in Figure 3.4.

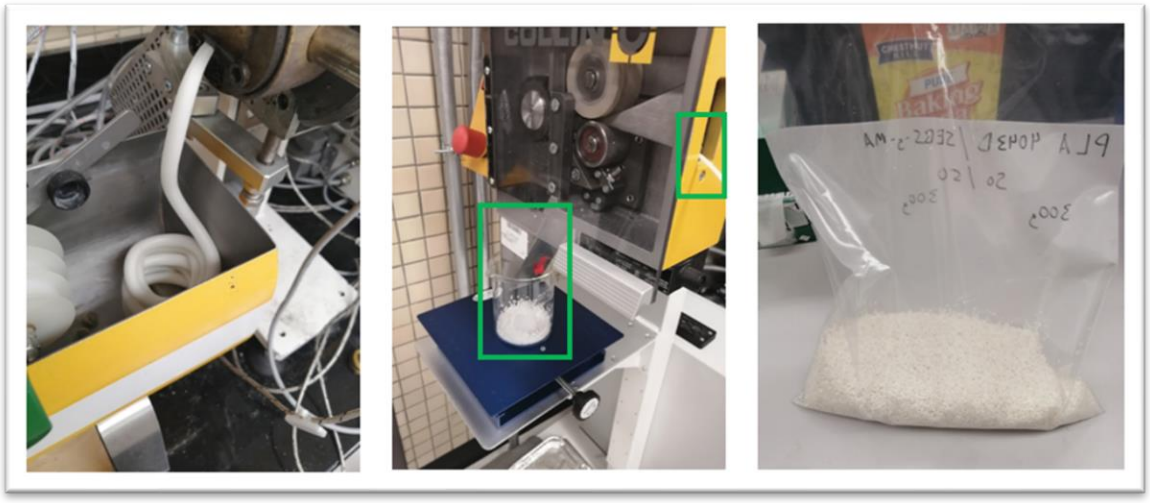

Figure 3.3 Extrusion & Pelletizing processes.

Figure 3.4 Final extruded filament.

Once the filament was created, the blend was checked for purity through the use of a Fourier Transform Infrared Spectrometer running in Attenuated Total Reflectance mode (FTIR-ATR). Figure 3.5 illustrates the equipment used (a spectrometer station FT-IR Nicolet iS5 model with an iD7 ATR, Thermo Fisher Scientific, Waltham Massachusetts).

Figure 3.5 Spectrometer (FT-IR Nicolet iS5 model with an iD7 ATR).

Chemical testing, in this case IR analysis, was extremely important to verify that there was contamination from other polymers (residue left over due to poor cleaning of the instrument) or even from the Dyna Purge used for purging (therefore it is important to leave this cleaning material flowing for 10 min and then observe the transition material which determines the start of the intended blend). Results were successful (this filament was compared to a previous batch of the same composition, from previous work by our lab which we are treating as a standard. The ATR Spectra is seen in Figures 3.6 and 3.7, the green boxes represent the peaks with differences in intensity as compared to the original analysis of the standard sample which confirms purity of the current batch. The name tags “extrusion batch end” and “extrusion batch hook” on Figures 3.6 & 3.7 are intended to differentiate the beginning and end of the extruded filament to verify any abnormality or contamination between the very beginning up to the final segment ejected from the extruder to confirm a consistency in the material. It should be noted that intensity difference does not correlate with a change in substance. Since there are no extra or missing peaks between the two spectra, we are confident that the material purity is sound.

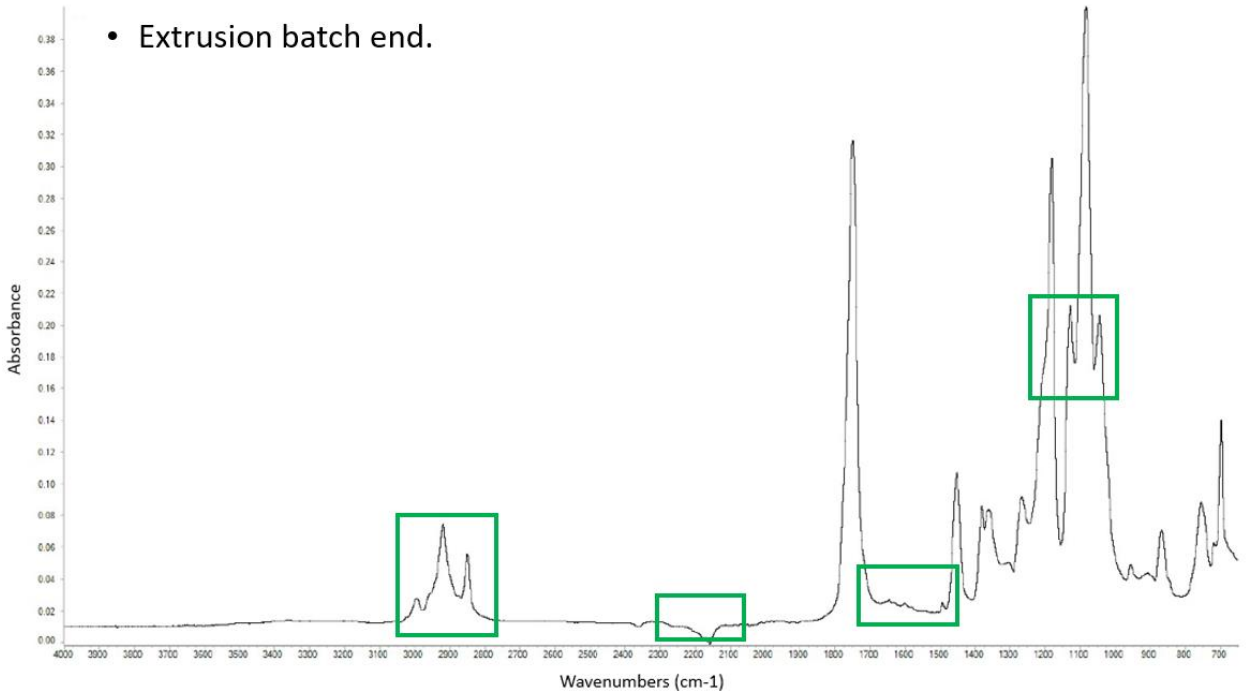

Figure 3.6 ATR Results (Extrusion batch end).

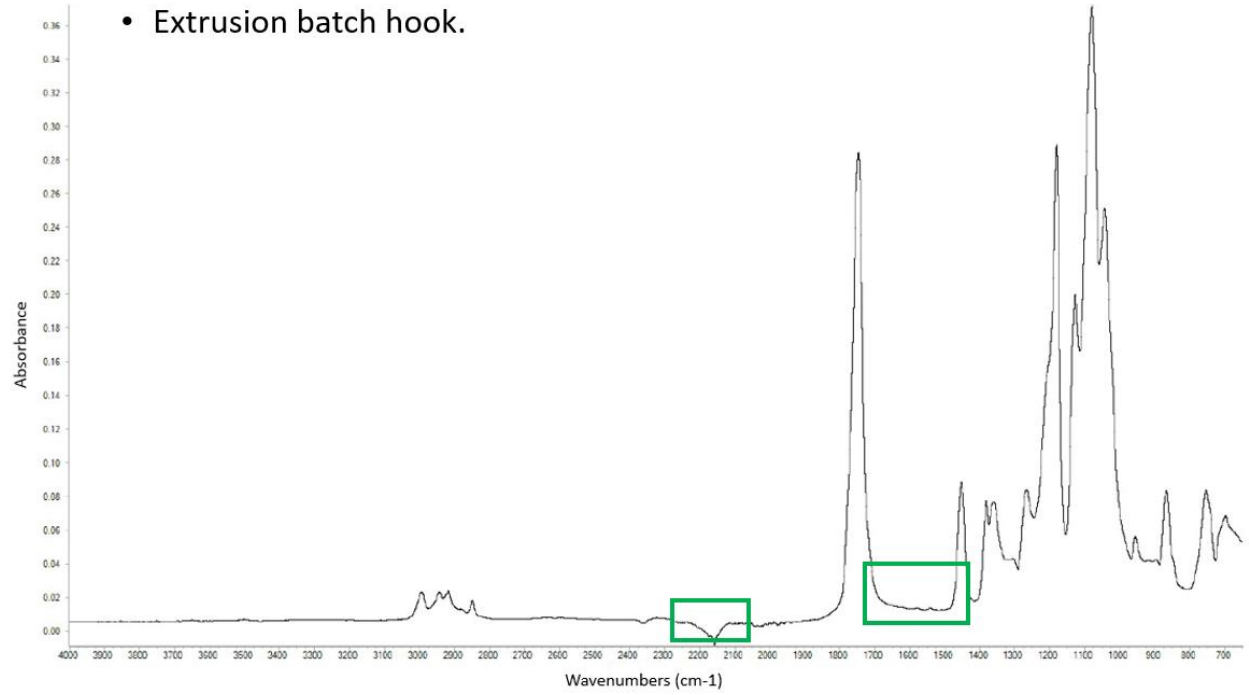

Figure 3.7ATR Results (Extrusion batch hook).

Once the ATR analysis proved our blend was pure, tensile test specimens were fabricated by FFF. Two specimens were fabricated to ascertain the maximum % elongation that could be sustained by the specimen. The ability to sustain at least 100% elongation is desired for the determination of shape memory properties. Figure 3.8 illustrates the equipment used for the tensile test, a Criterion C-44 equipped with an AHX 800 MTS High Elongation Extensometer, MTS Systems, Eden Prairie, MN). Figure 3.9 is a photograph of an example printed specimen. A full description of the specimen fabrication methodologies is explained further below.

Figure 3.8 MTS Criterion C-44.

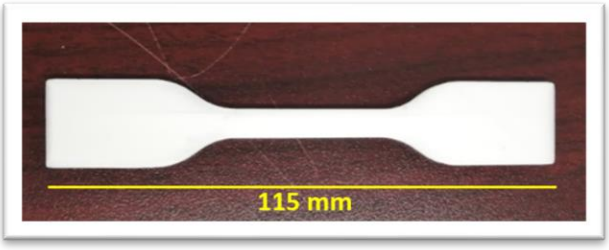

Figure 3.9 ASTM Type IV Longitudinal specimen fabricated by FFF.

Results from the initial mechanical testing of the polymer blend on both samples showed good response in that the specimens were able to sustain 100% elongation at room temperature. This let us know that the material was suitable for testing in the context of the determination of shape memory properties as well as the ability to ascertain the effect of environmental exposure on these properties. Figures 3.10, 3.11, 3.12 & Fig. 3.13 show the stress-strain curves of samples no. 1 & no. 2 graph results and visual break points, this helps to confirm and double-checked the quality of the materials.

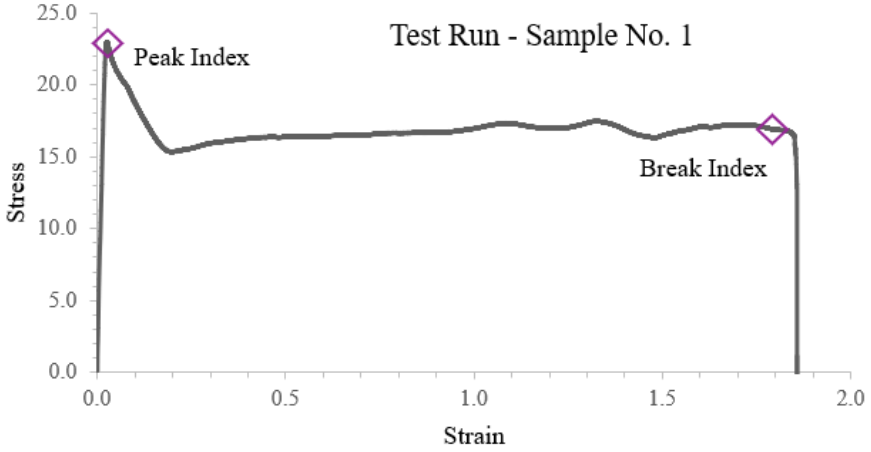

Figure 3.10 Stress vs. Strain graph results (Sample No.1).

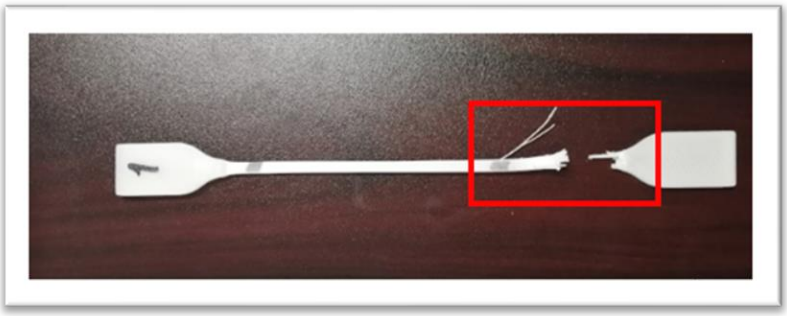

Figure 3.11 Sample No. 1 break point at 135.65 mm.

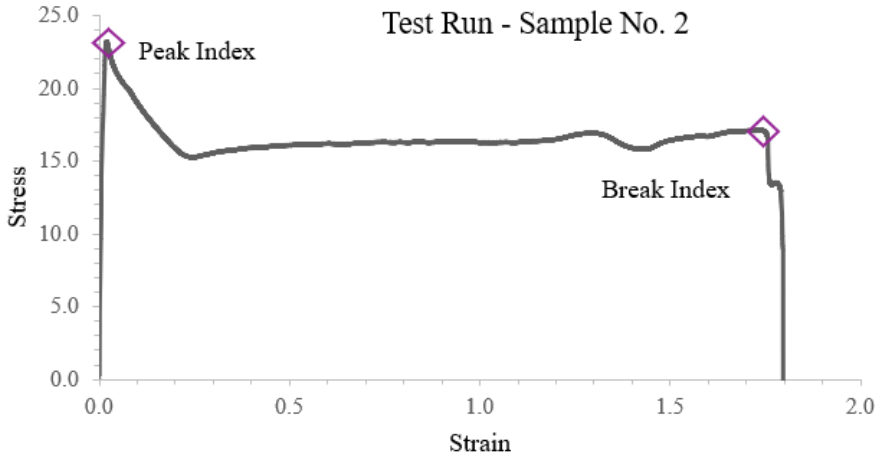

Figure 3.12 Stress vs. Strain graph results (Sample No.2).

Figure 3.13 Sample No. 2 break point at 136.05 mm.

3.1 Sample Manufacture

3.1.1 3D Printing Process

A total of 30 samples were fabricated by the FFF process using a Luzbot TAZ 5 (Luzbot, Fargo, North Dakota) with a 0.5mm nozzle as shown in Figure 3.14. Samples were stored on plastic zip bags with moisture absorber packs, to avoid any humidity concentration. Samples were fabricated in a longitudinal raster pattern where the print lines are parallel to the length of the

specimen. Figure 3.15 illustrates the horizontal raster pattern. 3D printing parameters are shown in Table 3-2.

Table 3-2 3D-Printing Parameters.

Material System	Pure PLA	PLA:SEBS
Ratio	NA	50:50
Nozzle Temp. (°C)	205	250
Bed Temp. (°C)	60	60
Printing speed (mm/s)	30	30

Figure 3.14 3D Printer Luzbot TAZ 5 3D.

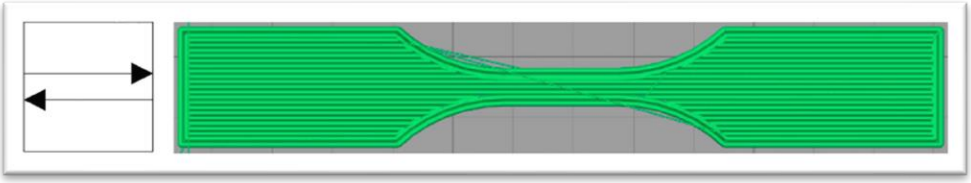

Figure 3.15 Schematic of the g-code filling pattern used: longitudinal, 0°

(Chávez, et al., 2019).

3.1.2 Plastic Injection Molding

Once the 3D printed samples were ready, the remaining of filament went through a pelletizing process, Figure 3.16 shows the equipment used (Pelletizer CDG 171/1, Collin Lab and Pilot Solutions, Norcross, GA, USA). Pelletization of the filament was needed so, the material could be processed in the manual plastic injection molded station as shown in Figure 3.17 (PIM-SHOOTER 150A, LNS Technologies, Scotts Valley, CA). In Table 3-3, injection parameters can be observed.

Figure 3.16 Pelletizer CDG 171/1.

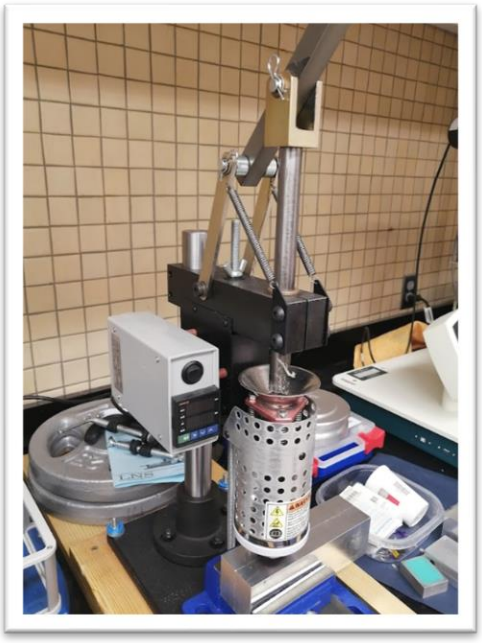

Figure 3.17 Manual plastic injection station (PIM-SHOOTER 150A).

Table 3-3 Plastic Injection Molding Parameters.

Material System	**PLA:SEBS**
Ratio	50:50
Injection Temp. (°C)	200

Specimens were injection molded at a temperature ranging between 392°F & 394°F (200°C & 201° C). After a waiting of 10 min (needed for temperature stabilization), the first manual shot was done, a constant manual pressure was needed to be maintained in order to concentrate the injection force into the mold and properly distribute the material. The mold used was machined from aluminum in the geometry of an ASTM D638 Type IV Tensile test specimen.

After the injection of the material, some of the samples presented burn marks from the interior of the injection cannon (please refer to Figure 3.18). These marks do not affect the

chemical or mechanical integrity of the material. Some samples were incomplete due to miscalculation of feed material, these samples were discarded.

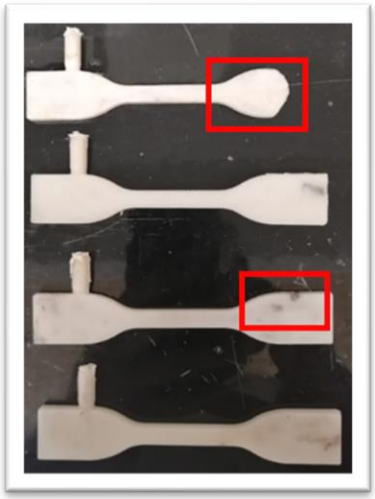

Figure 3.18 Burn marks of plastic injection molded samples.

3.6 Moisture Exposure

Prior to tensile testing, samples specified on Table 4-1 (Experimental Groups) in Chapter 4, that required moisture exposure, were submerged in DI water in a sealed glass container and set on a hotplate at 60°C with an exposure of 120 hours for every single group. After this procedure the specimens were left overnight at ambient temperature (25°C) over paper towels to remove excess or droplets of DI water. A weighing process was done before and after submersion for each sample to observe any liquid absorption variance. The precise scale use for these experiments was the VWR-123P AVANTOR (VWR RADNOR, PA). Figure 3.19 represents the process in which samples were moisture exposed. Figure 3.20 illustrates the weighing scale.

Figure 3.19 Sample submersion process.

Figure 3.20 VWR-123P (Weighing Machine).

CHAPTER 4: RESULTS AND DISCUSSION

4.1 Mechanical Testing - 3D Printed Specimens

The samples were divided into different groups for multiple testing as Table 4-1 illustrates. All documentation, results, and data can correlate and reviewed in an organized manner.

Table 4-1 Experimental Groups.

3D - Printed								Injection Molded			
Baseline				Moisture				Baseline		Moisture	
Pure PLA Pulled to failure	PLA/SEBS Pulled to failure	PLA/SEBS 100% Elongated	PLA/SEBS Annealed	Pure PLA Pulled to failure	PLA/SEBS Pulled to failure	PLA/SEBS 100% Elongated	PLA/SEBS Annealed	PLA/SEBS Pulled to failure	PLA/SEBS 100% Elongated	PLA/SEBS Pulled to failure	PLA/SEBS 100% Elongated

Environmental degradation was simulated by exposing the specimens to moisture (as main factor) and an elevated temperature. Exposed specimens were compared to baseline specimens and differences in the shape mechanical and shape memory properties were observed.

4.1.1 Pure PLA – Pulled to failure (Baseline)

The group consisted of three samples of pure PLA, these samples were submitted to complete failure by pulling the specimens until breakdown, also complete or partial ruptures were obtained as Figure 4.16 illustrates. The mechanical behavior shown by this material was of brittle nature, all samples broke instantly (even faster than the PLA-SEBS 50/50 blend). No high temperatures were used for this test group. Original length for all samples was 115 mm, no elongation was obtained.

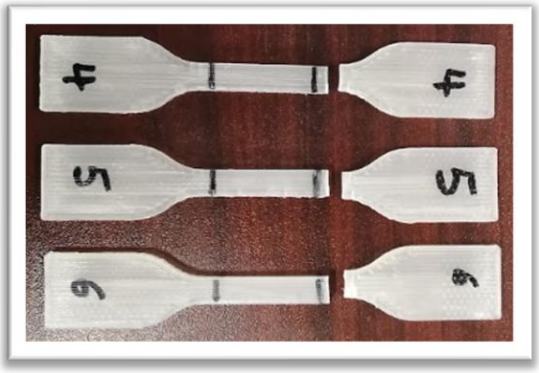

Figure 4.1 3D- Printed samples after being pulled to failure.

4.1.2 PLA-SEBS 50/50 – Pulled to failure (Baseline)

The baseline sample pool of five samples was pulled to failure, depending on the type of deformation (complete or partial ruptures). The gauge length of the samples was determined by measuring the entire length (individually), then diving this length by 2, and afterwards to the result, 12.7 mm were added in order to locate the distance of the first point mark. This served as a visual aid to physically mount the extensometer within the tensile tester (the other mark was drawn by using the mirror technique). Figures 4.2 & 4.3 show how the samples were prepared before the tensile test and the results after the breakpoint was reached.

Figure 4.2 PLA-SEBS 50/50 Pull to failure (Baseline) 3D-printed samples.

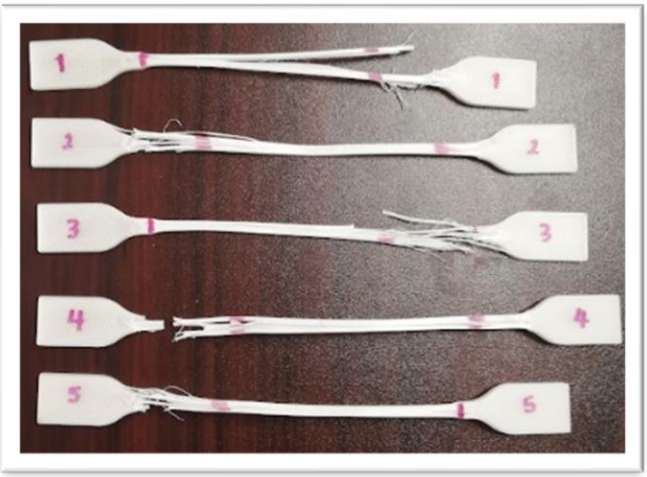

Figure 4.3 Samples after being pulled to failure.

4.1.3 PLA-SEBS 50/50 – Pulled to 100% - Recovered with heat – Pulled to failure (Baseline)

The purpose of this sample pool was to assess the difference in ultimate tensile strength that the material exhibits after being subjected to a shape memory process. The test group of five samples passed through different phases; The first one, consisted of pulling all the samples to a 100% elongation (no failure allowed). This was done manually by setting up the program to stop at a 25 mm extension. The test rate needed to be lowered from 12.7 mm/min (usual speed) to 6 mm/min due to the immediate failure of two samples (they were substituted by new ones). Figure 4.4 shows the samples as printed stated (including the samples that were exchanged). Once the samples were pulled to a 100% elongation, mechanical recovery was implemented by using heat. This is intended to contract the specimens to the original length and observe any possible mechanical change. The samples that failed before the decreasing of the test rate and the samples properly set to 100% elongation respectively are shown in Figure 4.5 a) & b).

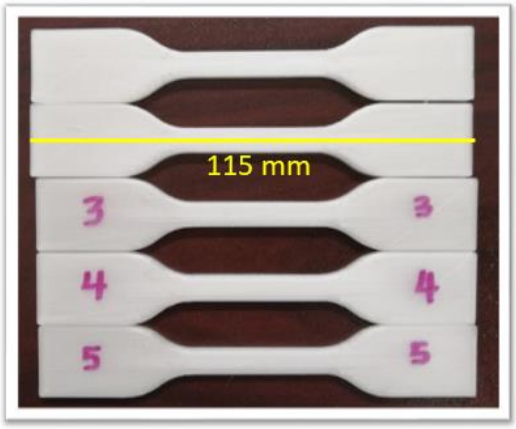

Figure 4.4 Samples as printed state.

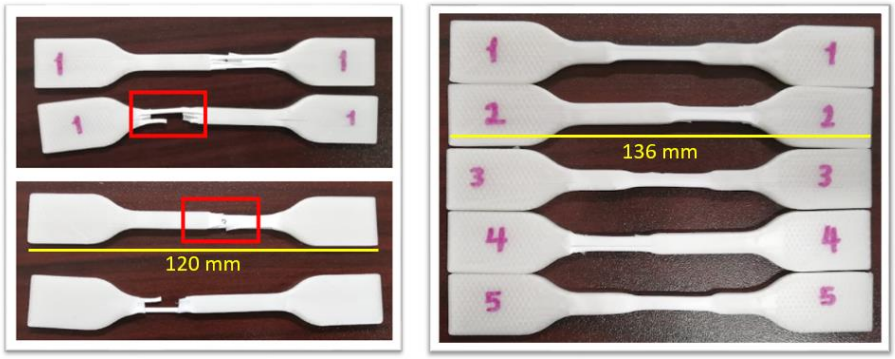

Figure 4.5 a) Fractured samples (12.7 mm/min rate) b) 100% elongated samples (6 mm/min rate)

The samples were introduced into a heating oven (VWR Oven F Air 3.65CF – Gravity Convection Oven, Radnor, PA) for a time lapse of 5 min at 70°C to recover their original structure [recovery temperature for PLA/SEBS 50:50 blend retrieved from (Paulina A. Quinonez, 2021)]. Once the heating cycle was ready, the samples were retreated. A significant observation can be made, not only length was restored, but also the marks made by the clamps of the tensile tester on the edges of the samples were vanished. To conclude the test, after the samples were retrieved from the oven, they were pulled to complete failure. Figures 4.6 & 4.7 show how the samples were prepared before the heating cycle was done. Figures 4.8 & 4.9 demonstrate the results of the mechanical recovery done to the samples after the heating cycle. As an important detail, samples

shrank 2 mm extra from their original length, this could have happened based on the time set. Figures 4.10 & 4.11 show how the samples were prepared before the tensile test and the results after they were pulled to complete failure.

Figure 4.6 Elongated samples prepared for heat recovery.

Figure 4.7 Elongated samples are set at the interior of the oven.

Figure 4.8 Samples moved due to mechanical recovery.

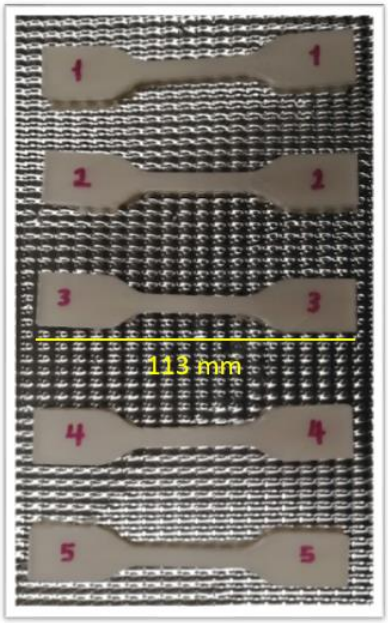

Figure 4.9 Samples with length recovered.

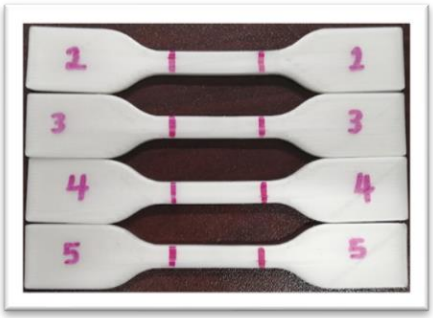

Figure 4.10 Heat recovered samples prepared for tensile testing.

Figure 4.11 Samples after being pulled to failure.

4.1.4 PLA-SEBS 50/50 – Annealed – Pulled to failure (Baseline)

Previously to the tensile test, the samples were exposed to heat for a time lapse of 5 min at 120°C (this temperature was suggested by Dr. David A. Roberson, taking into consideration previous results from DMA analysis taken from (Paulina A. Quinonez, 2021)). This was done to observe if high temperatures could affect mechanical properties. After the heating cycle, extreme shrinkage was observed. All samples were reduced in length and presented some side buckling. The test group of four samples was submitted to complete failure by pulling the specimens until breakdown, depending on the type of deformation, complete or partial ruptures were obtained. All samples broke immediately, showing brittle behavior. Figures 4.12 & 4.13 show the samples that have been set before the heating cycle and into the oven. Figures 4.14 & 4.15 demonstrate the

results of the samples after been heated and the setup before the tensile test. Figure 4.16 shows the result from the tensile test.

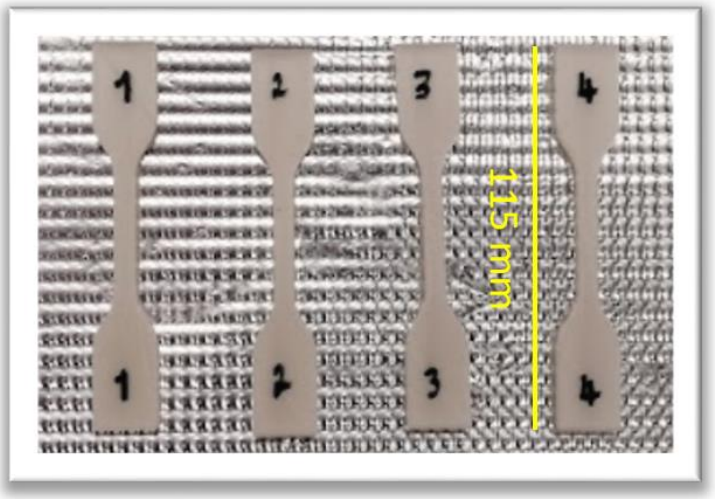

Figure 4.12 3D-printed samples before heating cycle.

Figure 4.13 Samples are set at the interior of the oven.

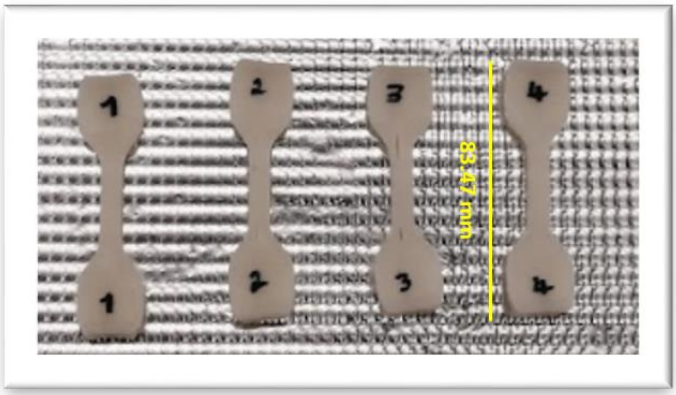

Figure 4.14 Shrank samples.

Figure 4.15 Samples set for tensile test.

Figure 4.16 Annealed samples after being pulled to failure.

4.1.5 Pure PLA – Pulled to failure (Moisture)

The moisture exposure sample group consisted of three samples of pure PLA. All specimens were put on a sealed container along with DI water as Figure 4.17 demonstrates. The hotplate was again set at 60°C and moisture exposure lasted for 120 hours. The weighing process was done before and after submersion as Table 4-2 shows the resulting weight values. Samples were also dried at ambient temperature. Specimens were pulled to failure. Figures 4.18 & 4.19 show the samples before and after the tensile test. Brittle behavior was encountered as baseline group.

Figure 4.17 Pure PLA 3D-printed samples are set for submersion process.

Table 4-2 Pure PLA - Pulled to Failure (Moisture) samples - Before & After weights.

Sample	Before	After
1	6.400 g.	7.370 g.
2	6.164 g.	6.570 g.

3	7.285 g.	7.378 g.

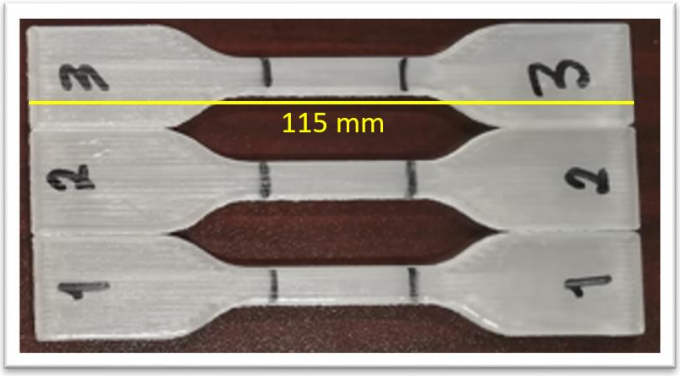

Figure 4.18 Samples set for tensile test.

Figure 4.19 Samples after being pulled to failure.

4.1.6 PLA-SEBS 50/50 – Pulled to failure (Moisture)

The test group of blend specimens exposed to moisture consisted of four samples. Figure 4.20 shows the numbered samples and their length reference.

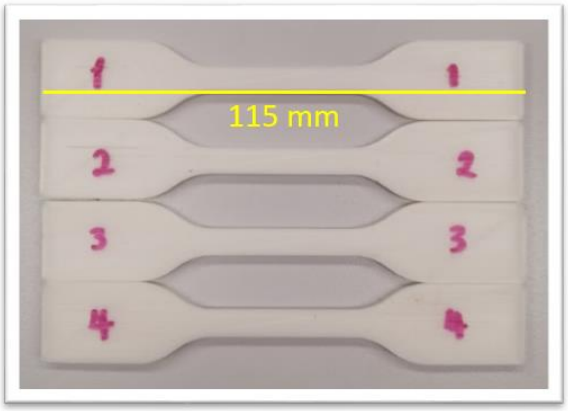

Figure 4.20 3D-printed samples numbered before moisture exposure.

Figures 4.21 shows the equipment setup used. Table 4-3 shows the weight values before and after moisture exposure. Samples showed very low moisture absorption. When drying was finished, all samples were pulled to failure. All samples were set for tensile testing as Figure 4.22 demonstrates. Figures 4.23 & 4.24 show the results from the tensile test and the different ruptures.

Figure 4.21 Sample submersion process.

Table 4-3 PLA-SEBS 50/50 Pulled to failure (Moisture) samples - Before & After weights.

Sample	Before	After
1	4.947 g.	5.018 g.
2	4.962 g.	5.043 g.
3	4.950 g.	5.069 g.
4	5.050 g.	5.135 g.

Figure 4.22 Samples prepared before tensile testing.

Figure 4.23 Samples 1 & 2 after being pulled to failure.

Figure 4.24 Samples 3 & 4 after being pulled to failure.

4.1.7 PLA-SEBS 50/50 – Pulled to 100% - Recovered with heat – Pulled to failure (Moisture)

The group consisted of four samples; they were all DI water exposed. The purpose of this sample pool was to understand the effect of moisture on the shape memory and self-healing properties of this material system. Figure 4.25 illustrates the submersion process of the samples. Specimens were dried using the same procedure at ambient temperature. Table 4-4 shows the resulting weight values. Samples were set to an 100% elongation at the tensile tester. Figures 4.26 & 4.27 show the samples length before and after elongation. All specimens were submitted to heat recovery at 70°C for 5 minutes as Figure 4.28 demonstrates the specimens set inside the oven. Afterwards, samples were set to the final tensile test. Figures 4.29 and 4.30 show the samples before and after being pulled to failure respectively.

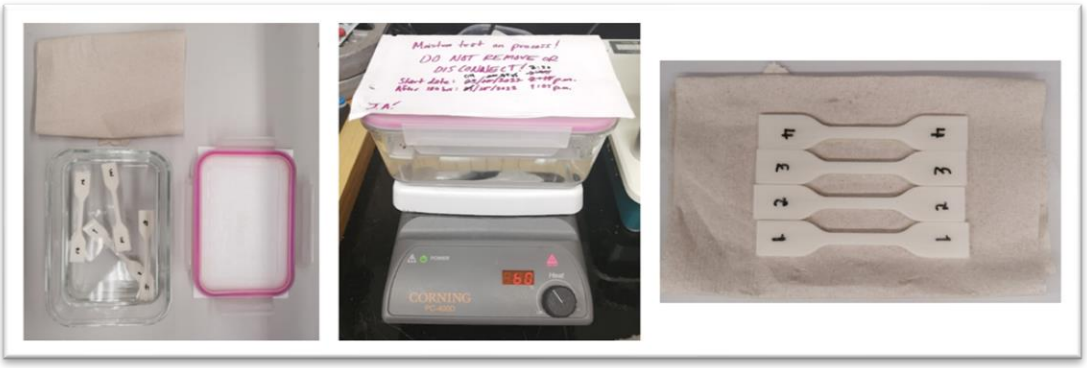

Figure 4.25 Sample submersion process.

Table 4-4 PLA-SEBS 50/50 Pulled to 100% - Recovered with Heat- Pulled to Failure (Moisture) samples - Before & After weights.

Sample	Before	After
1	4.927 g.	4.986 g.
2	4.987 g.	5.034 g.
3	4.993 g.	5.047 g.
4	5.145 g.	5.192 g.

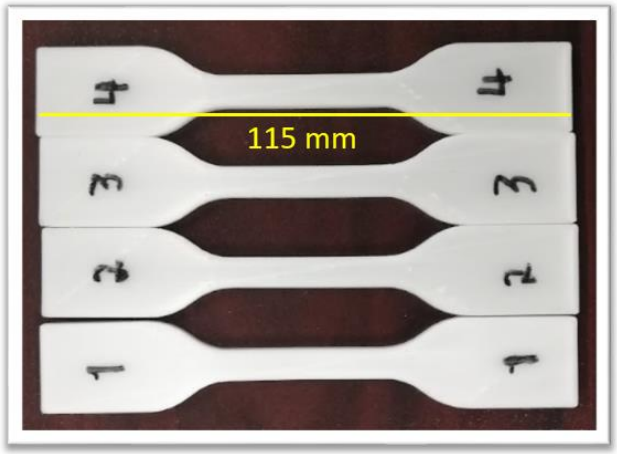

Figure 4.26 3D-printed samples before 100% elongation.

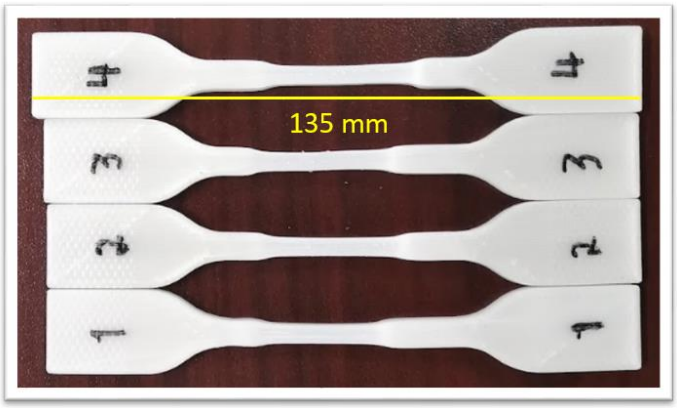

Figure 4.27 Samples after 100% elongation.

Figure 4.28 Samples set at interior of the oven at 70°C.

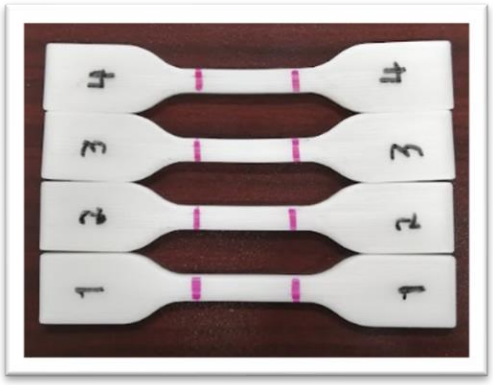

Figure 4.29 Samples prepared for tensile test after heat recovery.

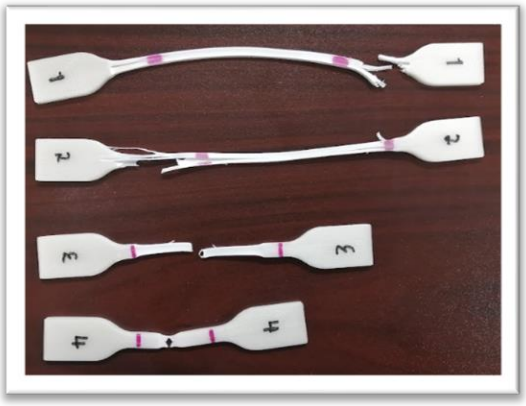

Figure 4.30 Samples after being pulled to failure.

4.1.8 PLA-SEBS 50/50 – Annealed – Pulled to failure (Moisture)

The group was formed by four samples of 115 mm length. They were annealed at 120°C for 5 minutes before water exposure. Figure 4.31 shows the samples been taken out from the oven. Figure 4.32 demonstrates the submersion process. Samples were dried at ambient temperature. Table 4-5 shows the resulting weight values. Extreme shrinkage was observed, same as the baseline group. Samples were pulled to failure. Figures 4.33 & 4.34 show the samples before/after the tensile test. Brittle behavior was encountered.

Figure 4.31 3D-printed samples been taken from the oven.

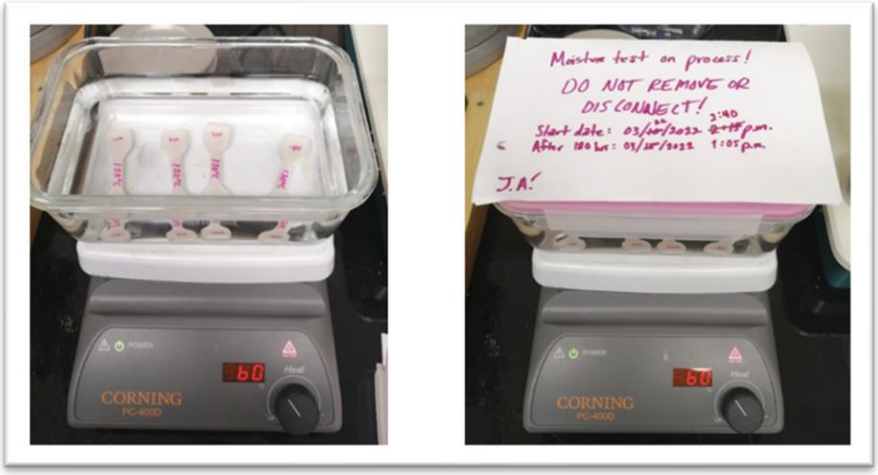

Figure 4.32 Samples submersion process.

Table 4-5 PLA-SEBS 50/50 Annealed - Pulled to Failure (Moisture) samples - Before & After weights.

Sample	Before	After
1	5.043 g.	5.096 g.
2	5.213 g.	5.257 g.

3	4.921 g.	4.985 g.
4	4.900 g.	4.971 g.

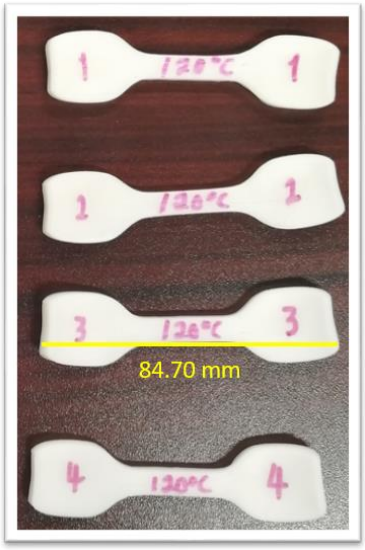

Figure 4.33 Samples with extreme shrinkage.

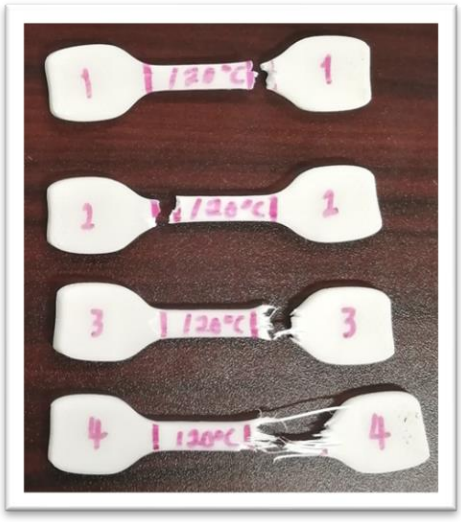

Figure 4.34 Samples after being pulled to failure.

4.2 Mechanical Testing - Plastic Injection Molded Specimens

As was the case with the 3D printed samples, the injection molded specimens were submitted to different environmental conditions. Eight samples were exposed to moisture and the rest of them left as the baseline group. All the samples were pulled to failure.

4.2.1 PLA/SEBS 50:50 – Pulled to Failure (Baseline)

The test group was made by three specimens, they were submitted to complete failure by pulling the specimens until breakdown, complete ruptures were obtained. Samples were measured by locating the first point mark that served as a visual aid to physically mount the extensometer within the tensile tester (the other mark was drawn by using the mirror technique). As a main observation, samples showed extreme brittle behavior. This can be directly associated to the high temperature exposure previously set from the samples manufacturing process. Figures 4.35 & 4.36 show the samples before and after the tensile test and the final ruptures.

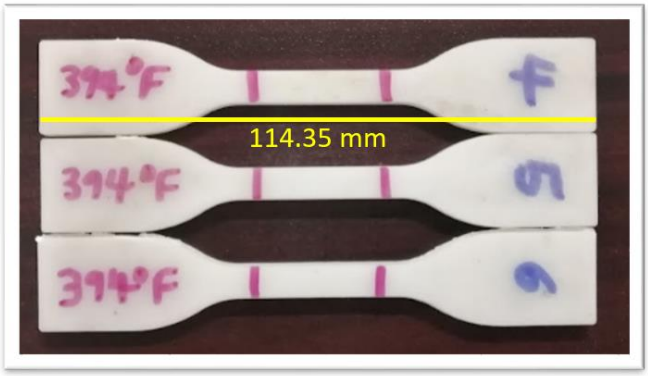

Figure 4.35 PLA-SEBS 50/50 plastic injection molded samples set for tensile test.

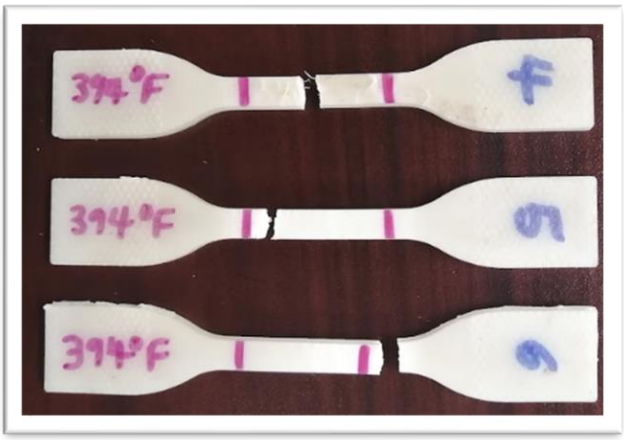

Figure 4.36 Samples after being pulled to failure.

4.2.2 PLA/SEBS 50:50 – Pulled to Failure (Moisture)

The group was formed by three samples. A sealed container was used along with DI water as Figure 4.37 demonstrates. Table 4-6 shows weight values. Specimens were also dried at ambient temperature. Samples were submitted to direct failure on the tensile tester. Figures 4.38 & 4.39 show the samples before and after the tensile test. Extreme brittle behavior was encountered.

Figure 4.37 Samples submersion process.

Table 4-6 PLA-SEBS 50/50 Pulled to Failure (Moisture) samples - Before & After weights.

Sample	Before	After
1	6.086 g.	6.897 g.
2	7.232 g.	7.320 g.
3	7.471 g.	7.539 g.

Figure 4.38 Plastic injection molded samples set for tensile testing.

Figure 4.39 Samples after being pulled to failure.

4.2.3 PLA-SEBS 50/50 – Pulled to 100% - Recovered with heat – Pulled to failure (Baseline)

The group consisted of five samples. Samples were set to an 100% elongation at the tensile tester. All specimens were submitted to heat recovery at 70°C for 5 minutes inside the oven. Subsequently, samples were set to the final tensile test.

4.2.4 PLA-SEBS 50/50 – Pulled to 100% - Recovered with heat – Pulled to failure (Moisture)

The group consisted of five samples; they were all DI water exposed. Specimens were dried using the same procedure at ambient temperature. Table 4-7 shows the resulting weight values. Samples were set to an 100% elongation at the tensile tester. All specimens were submitted to heat recovery at 70°C for 5 minutes inside the oven. Afterwards, samples were set to the final tensile test.

Table 4-7 PLA-SEBS 50/50 Pulled to 100% - Recovered with Heat- Pulled to Failure (Moisture) samples - Before & After weights.

Sample	Before	After
1	6.582 g.	6.619 g.
2	6.718 g.	6.741 g.
3	6.656 g.	6.687 g.
4	6.625 g.	6.649 g.
5	6.607 g.	6.648 g.

4.3 Tensile Analysis

Tensile analysis of the materials studied in this research was performed to determine the tensile properties of the shape memory polymers as well as to determine which material systems had their properties affected based on the moisture and temperature exposure. The UTS and % elongation values were compared based on the sample manufacturing process and environmental testing in Figures 4.40 - 4.43. The plots presented below from Figures 4.40 - 4.43 are representative data values from each material composition and sample group.

4.3.1 3D-Printed Samples (Baseline & Moisture Groups)

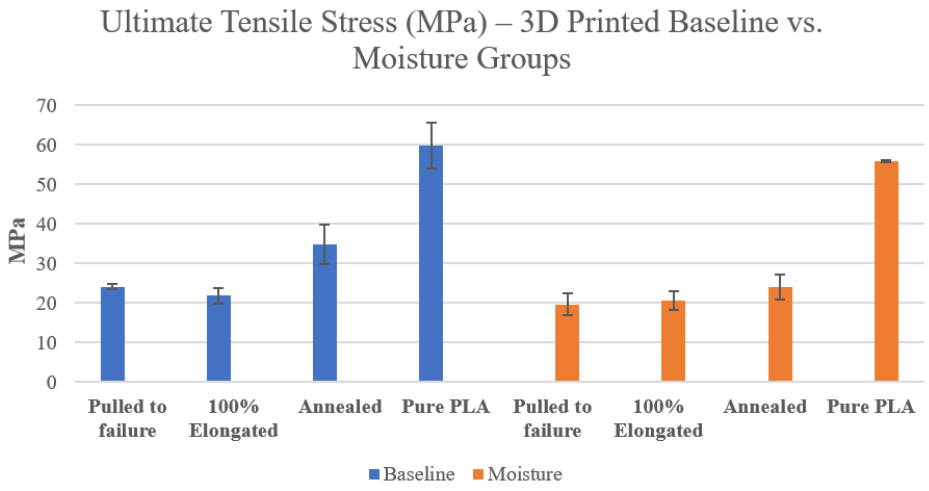

Figure 4.40 UTS Average Plots of the 3D Printed Sample Groups.

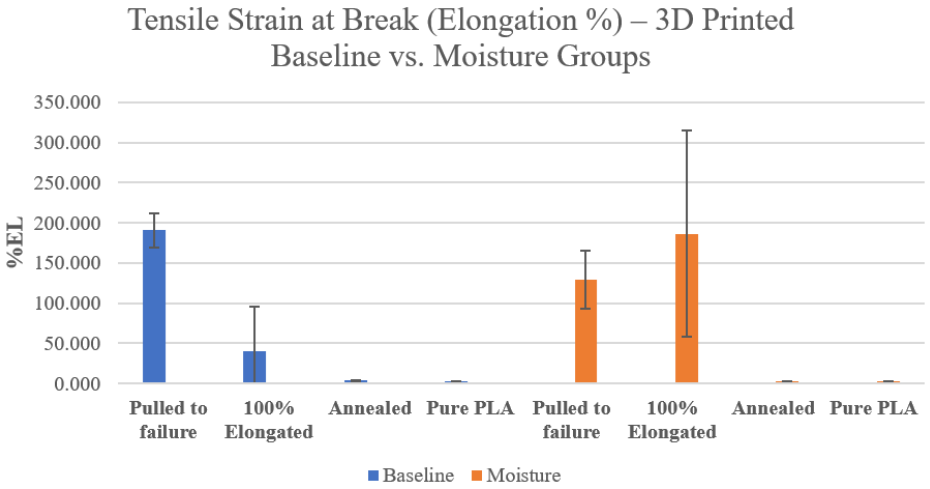

Figure 4.41 % Elongation Average Plots of the 3D Printed Sample Groups.

4.3.2 Plastic Injection Molded Samples (Baseline & Moisture Groups)

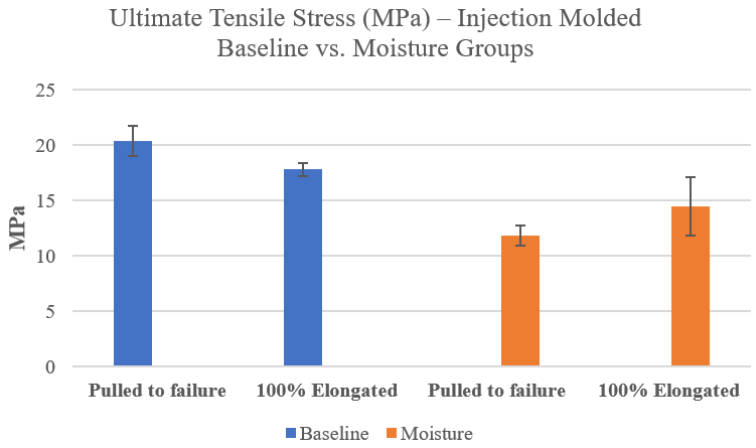

Figure 4.42 UTS Average Plots of the Injection Molded Sample Groups.

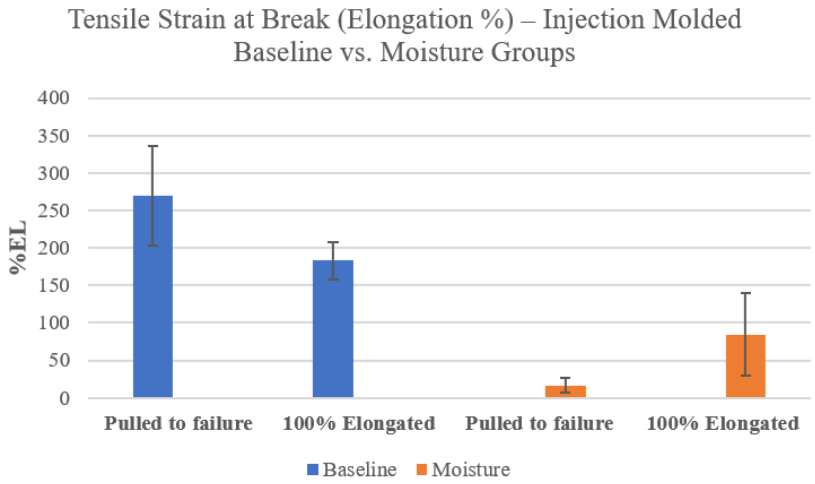

Figure 4.43 % Elongation Average Plots of the Injection Molded Sample Groups.

4.4 Data Comparison

4.4.1 Stress at Yield

The stress at yield values were higher for 3D-printed specimens that were not exposed to moisture as compared to those that were exposed. Injection molded specimens submitted to moisture exhibited lower stress values as compared to baseline samples, indicating that water

submersion led to a decrease in mechanical properties. Figures 4.44 & 4.45 show the 3D-printed and mold injected specimens' visual data for the stress at yield values.

3D-Printed Specimens

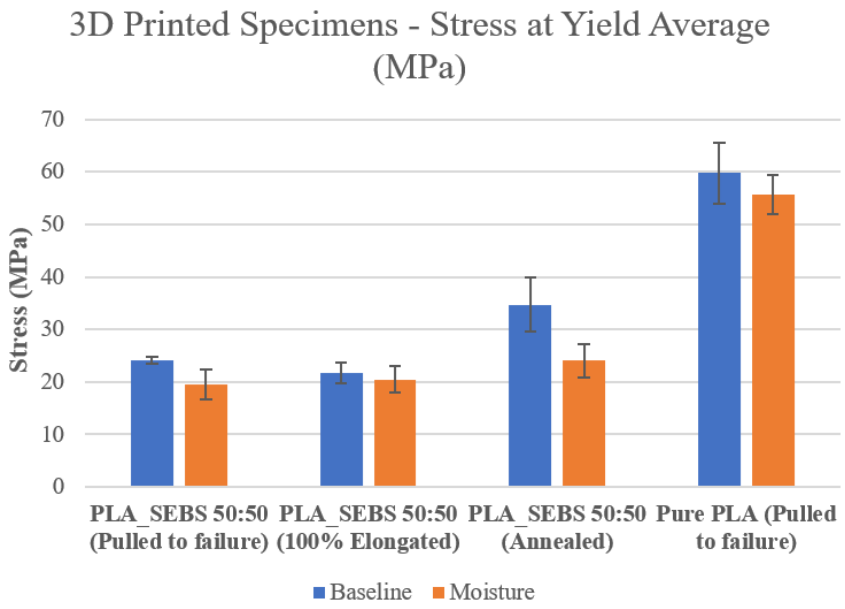

Figure 4.44 3D-Printed specimens' average forces (n=30); Stress at yield average.

Plastic Injection Molded Specimens

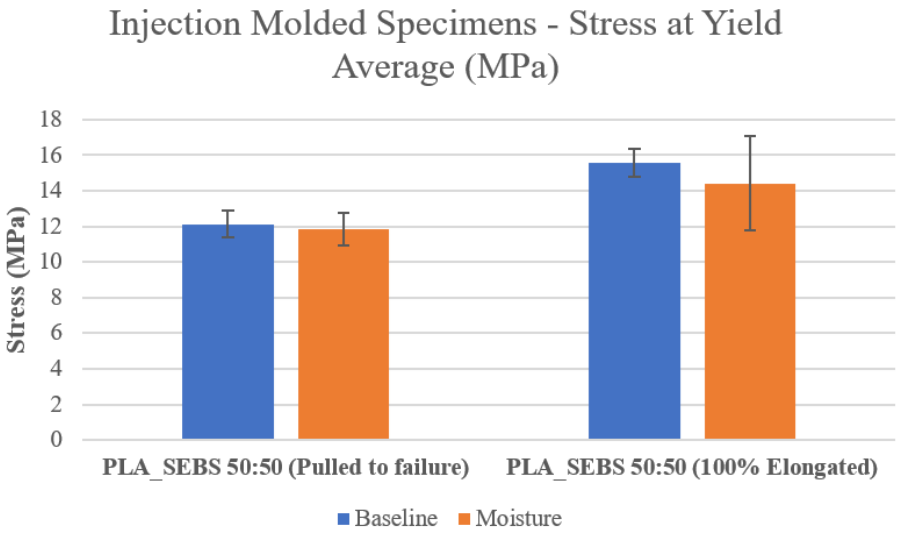

Figure 4.45 Injection molded specimens' average forces (n=18); Stress at yield average.

4.4.2 Heat Recovery Comparison for 100% Elongated Specimens

In terms of comparing the fixation ratio and recovery ratio for the groups exposed and not exposed to moisture, the 3D-printed samples that were previously submitted to humidity obtained a higher percentage of fixation than the baseline specimens, but recovery resulted higher in the specimens not exposed to moisture. In contrast, for the injection molded samples, fixation and recovery was lower for the specimens submitted to moisture in comparison to the baseline specimens. In Figure 4.46, the visual comparison data from the baseline and moisture groups can be observed.

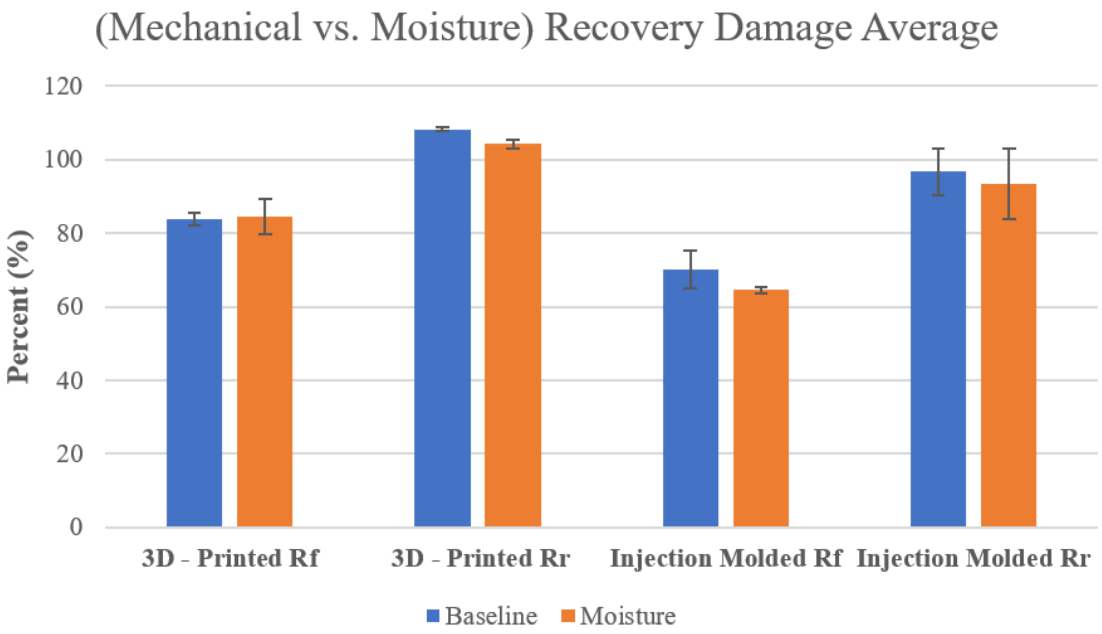

Figure 4.46 Comparison between the mechanical and moisture recovery tensile groups.

4.5 Fracture surface analysis

4.5.1 3D-Printed Specimens

Scanning electron microscopy (SEM) microanalysis of the fracture surfaces of representative specimens from the PLA/SEBS 50:50 blend system revealed that the fracture mode

changes based on thermomechanical history. The pure PLA specimens exhibited a purely brittle mode failure. All images were taken from the breakpoint area of the rupture to enable comparison of the fracture surfaces. Starting with Figure 4.47 a), a PLA/SEBS 50:50 baseline specimen submitted to direct failure, the sample had a partial break, where a dominant feature is the delamination of the print rasters. The fracture surface morphology (Fig. 4.47 a and b) is that of ductile mode failure characterized by an absence of craze cracking and a large amount of plastic deformation. The fracture surfaces in Figure 4.47 c) & d) correspond to a PLA/SEBS 50:50 specimen pulled to a 100% elongation, recovered with heat, and then pulled to complete failure. The fracture surface morphology is different as compared to the baseline specimens. In Figure 4.47 d) multiple layers can be observed confirming that the fiber indicating that less delamination of the print occurred. Lateral delamination did occur to the point that the individual print layers can be seen as highlighted by arrows in Fig. 4.47 c). Rather than a large amount of plastic deformation fracture surfaces resembling craze cracks manifested characterized by ridges where one is highlighted by a white arrow in Fig. 4.47 d). The fracture plane is more planar than the baseline specimen and more consistent with a brittle mode failure. Similar fracture surfaces have been observed by (Siqueiros, J. Gilberto; Schnittker, Kevin & Roberson, David A., 2016) for similar material systems and indicated that the cross-sectional area loss due to the necking of a specimen led to the manifestation of fracture morphology that resembled the fracture surface of a brittle material thought the material was ductile due to the large amount of elastomer content.

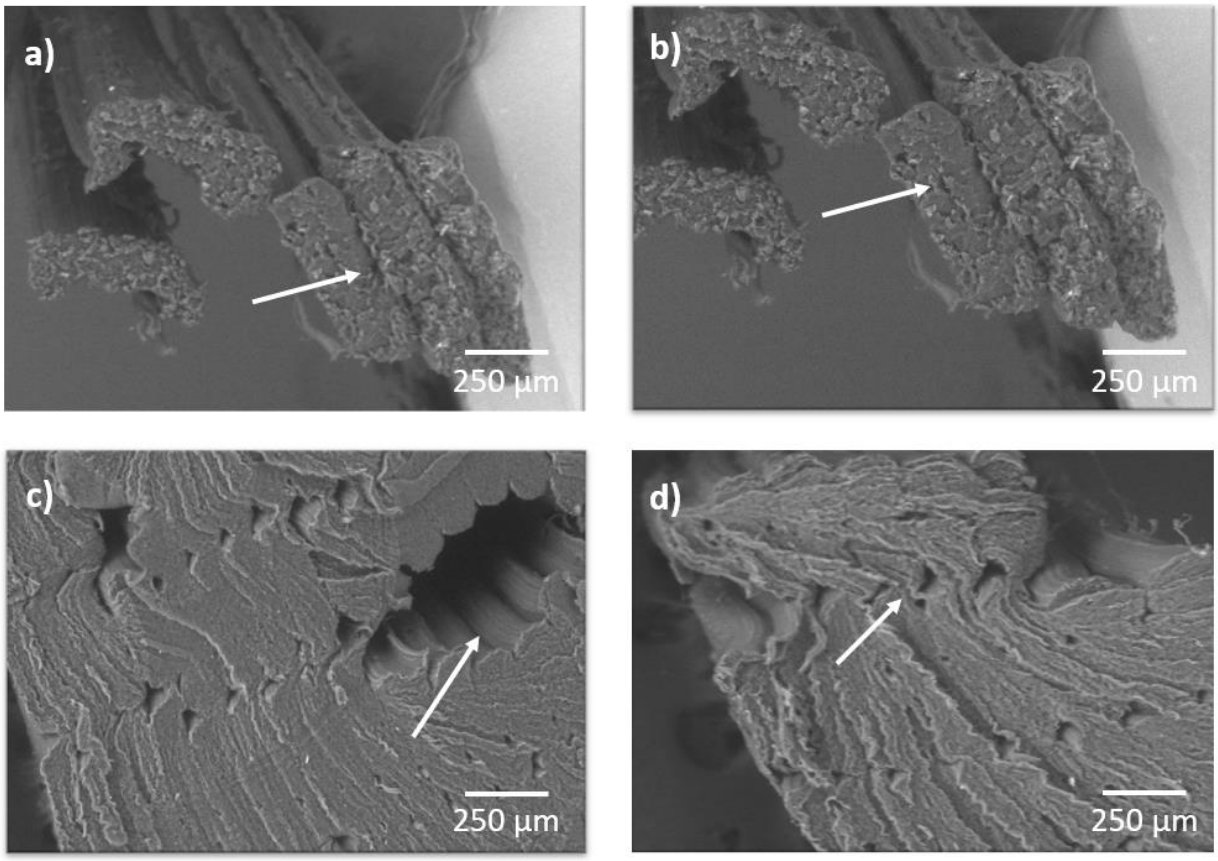

Figure 4.47 SEM Micrographs of tensile fracture surfaces of PLA/SEBS 50:50 Baseline for a) & b) Pulled to failure and c) & d) Pulled to failure after thermally recovering from 100% elongation in a shape memory process (Bottom and Top).

The following images indicate that the fracture surface for PLA/SEBS 50:50 baseline annealed and pulled to failure specimens changes drastically when temperature is increased and provides information related to the thermal post-processing of this material. All images of the PLA/SEBS 50:50 printed system were taken at the same magnification using BSE (backscattered electrons). Figure 4.48 a) shows plastic deformation at the surface and bonding between 3D printed layers within the specimen can be observed. Fibers can be looked on the entire area of the break detection, result from the crystallization of the specimen. In Figure 4.48 b) similar behavior is encountered on the other side of the sample; steps, and fibrils are also present. Though the

annealing process had the negative impact of shrinking the specimens, the thermal processing negated delamination of the print rasters and allowed the material to behave as a ductile elastomeric would be expected to. The fracture surfaces of baseline PLA specimens (Fig 4.48 c and d) exhibit a typical brittle failure mode characterized by a low amount of plastic deformation and ridges due to craze crack formation.

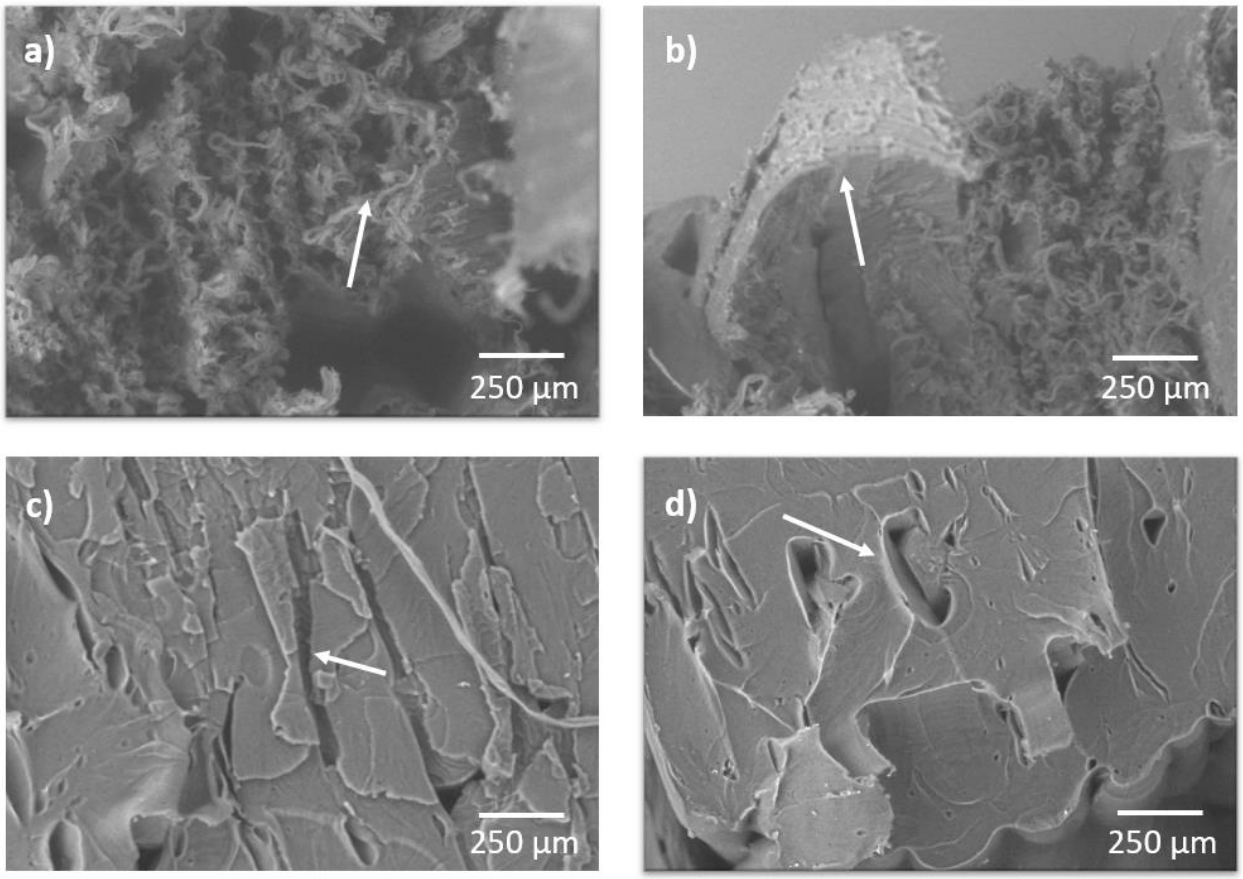

Figure 4.48 SEM Micrographs of tensile fracture surfaces of PLA/SEBS 50:50 Baseline for a) & b) Pulled to failure after annealing and Pure PLA Baseline for c) & d) Pulled to failure.

Fracture surface analysis of PLA/SEBS 50:50 moisture specimens pulled to failure was also viewed under SEM to determine the fracture characteristics with increasing humidity exposure. The image seen in Figure 4.49 a) demonstrates more plastic deformation and fibrils in the break area. Moisture increased the plasticity of the specimens. The exposure to moisture at an elevated temperature effectively plasticized the material, most-likely the PLA component of the

blend, leading to a greater amount of plastic deformation. Figure 4.49 b) shows that fibrils formed in groups as indicated by the feature pointed out by the white arrow. As for Figures 4.49 c) & d), PLA/SEBS 50:50 pulled to a 100% elongation, recovered with heat, and then pulled to complete failure samples indicate that less plastic deformation occurred prior to rupture. Delamination of the print rasters occurred where one segment is indicated by the white arrow in 4.49 c) and the arrow in 4.49 d) indicated the print rasters made visible by lateral delamination.

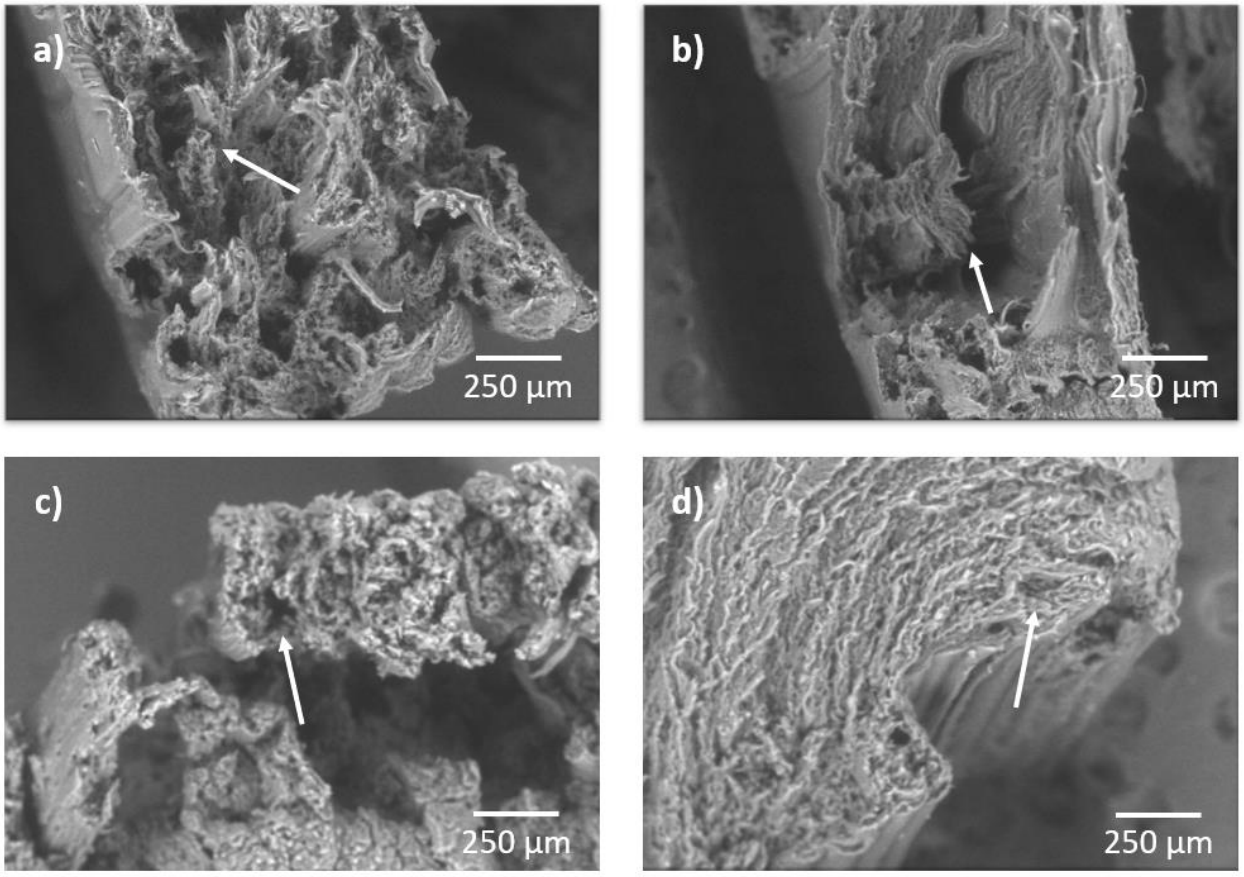

Figure 4.49 SEM Micrographs of tensile fracture surfaces of PLA/SEBS 50:50 Moisture for a) & b) Pulled to failure and c) & d) Pulled to failure after thermally recovering from 100% elongation in a shape memory process.

The surface fracture area for this PLA/SEBS 50:50 moisture annealed and pulled to failure specimen analysis also exhibited brittle mode failure. A large fibril is indicated by the white arrow

in Figure 4.50 a) while the arrow in Figure 4.50 b) indicated a print raster void characteristic of the FFF process that is surrounded by a cluster of fibrils. For the PLA moisture pulled to failure specimen, Figures 4.50 c) & d) show that the sample has same behavior as the baseline specimen. Moisture did does not affect the fracture behavior which was dominated by brittle fracture features nature along with crazing zones. Fabrication-related features are indicated by the white arrows in Figure 4.50 c) and 4.50 d), respectively.

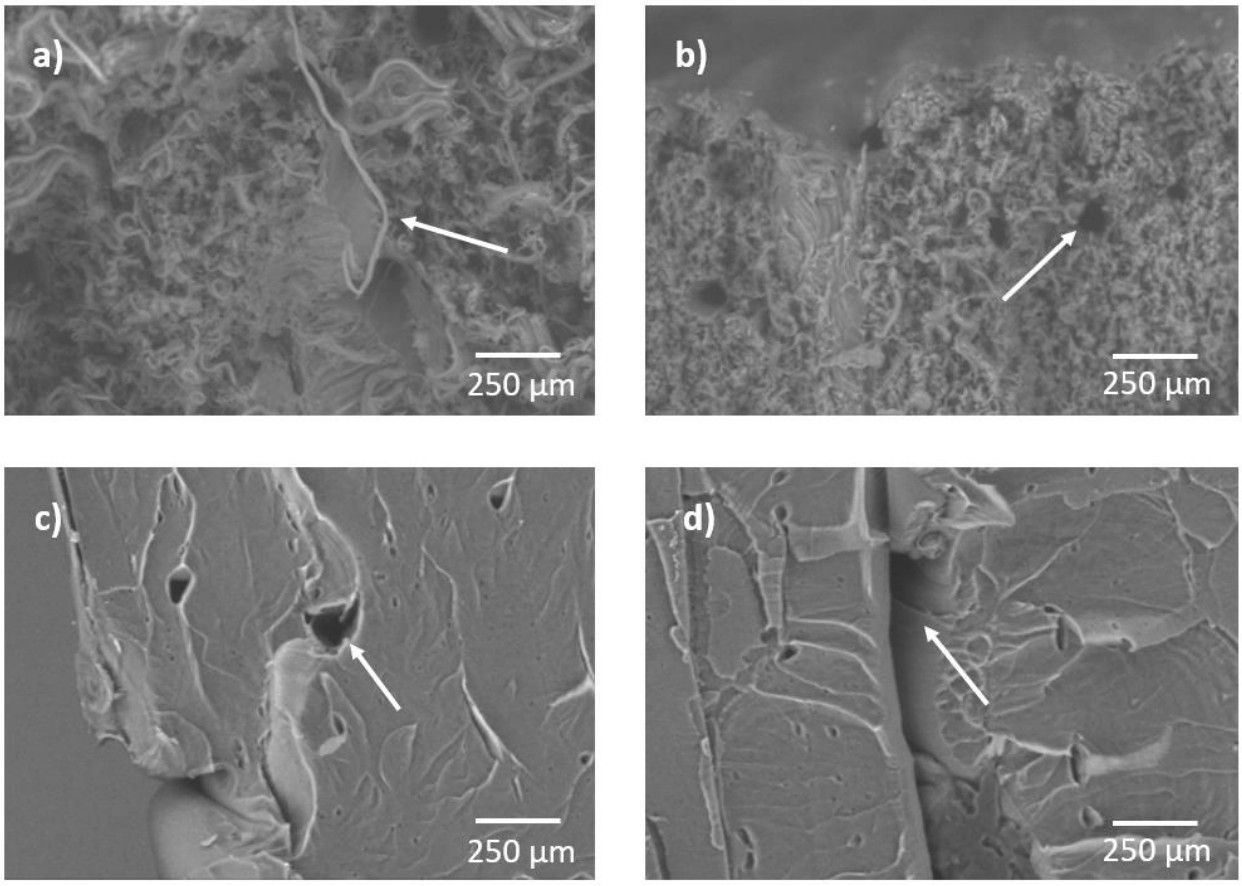

Figure 4.50 SEM Micrographs of tensile fracture surfaces of PLA/SEBS 50:50 Moisture for a) & b) Pulled to failure after annealing and Pure PLA Moisture for c) & d) Pulled to failure.

4.5.2 Injection Molded Specimens

Fracture surface analysis of injection molded specimens was also viewed under SEM to determine the fracture characteristics associated with the fabrication process. The images below for the PLA/SEBS 50:50 injection molding systems were taken for both the baseline, and moisture exposed samples. Figure 4.51 a) shows that the fracture surface is dominated by fibrils. Without defects associated with the FFF manufacturing process, there is no delamination, and a better indication of bulk material performance can be observed. In Figure 4.51 b) it can be seen that fibrils all over the fracture surface. Similar fracture morphology is observed for the specimen subjected to moisture and then pulled to failure (Fig. 4.51 c and d). For Figures 4.51 c) & d) the presence of fibrils is highlighted.

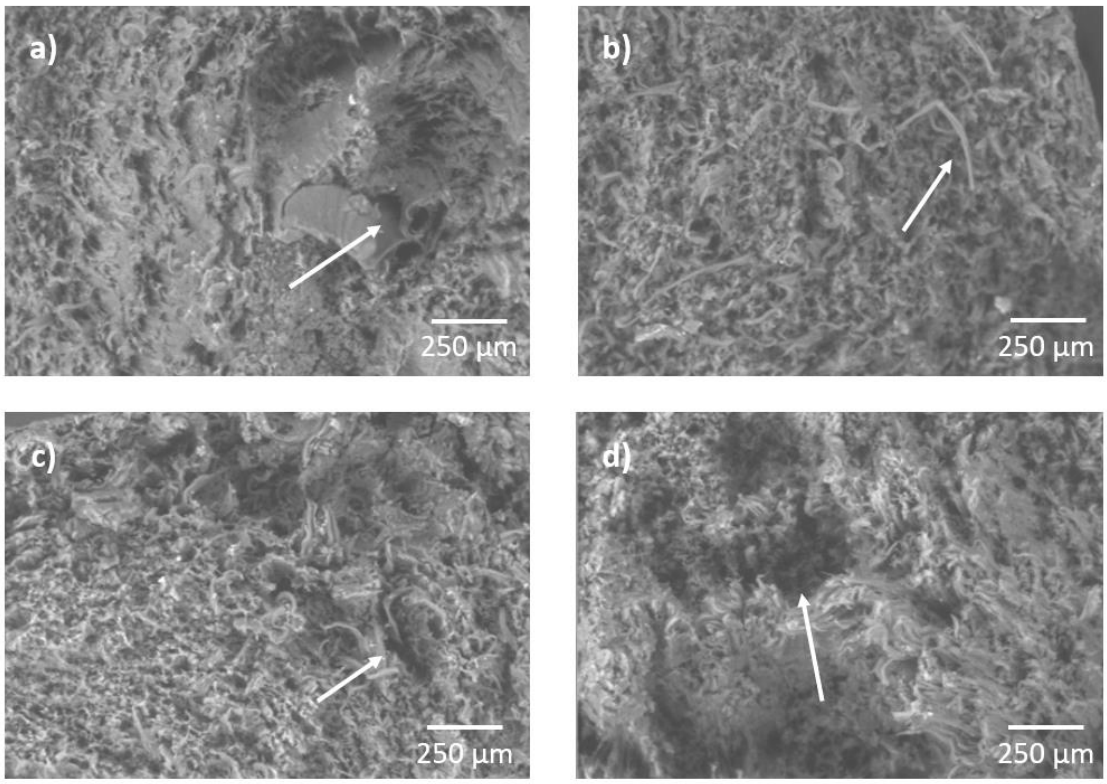

Figure 4.51 SEM Micrographs of tensile fracture surfaces of plastic injection molded PLA/SEBS 50:50 Baseline for a) & b) Pulled to failure and PLA/SEBS 50:50 Moisture for c) & d) Pulled to failure.

4.6 XRD Analysis

Analysis of the specimens via X-Ray diffraction (XRD) revealed that all blends composed of PLA: SEBS are amorphous in the as-printed state. PLA alone is known to be heat-treatable to the point of inducing crystallinity. The characteristic peaks associated with PLA can be seen where the most prominent peak is, the (110)/(200) XRD spectra for PLA 4043D at 16.9 degrees at an annealed condition, information retrieved from (Diego Bermudez; Paulina A. Quinonez; Evelin J. Vasquez; Israel A. Carrete; Truman J. Word & David A. Roberson, 2021).

XRD spectrums can be seen in Figures 4.52 & 4.53. The spectra also show the amorphous halo that is present roughly between 10 and 24 degrees on the 2θ scale. As an observation, made in this study, was that the blend systems submitted to high temperatures exhibited crystallinity after as indicated by the peaks.

PLA-SEBS 50/50 – Baseline 3D-Printed Annealed Specimen

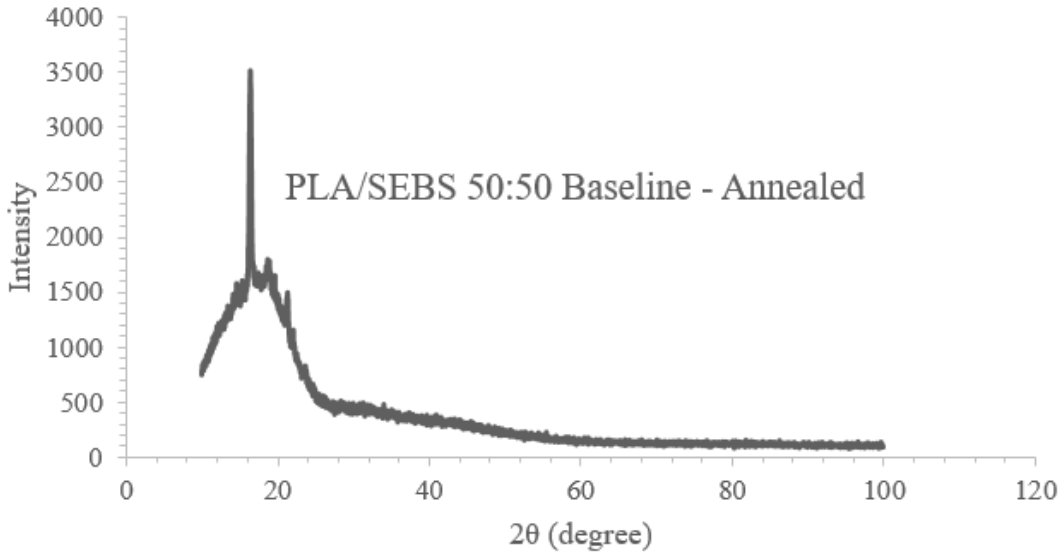

Figure 4.52 XRD spectra for the PLA-SEBS 50/50 – Baseline Annealed Specimen.

PLA-SEBS 50/50 – Moisture 3D-Printed Annealed Specimen

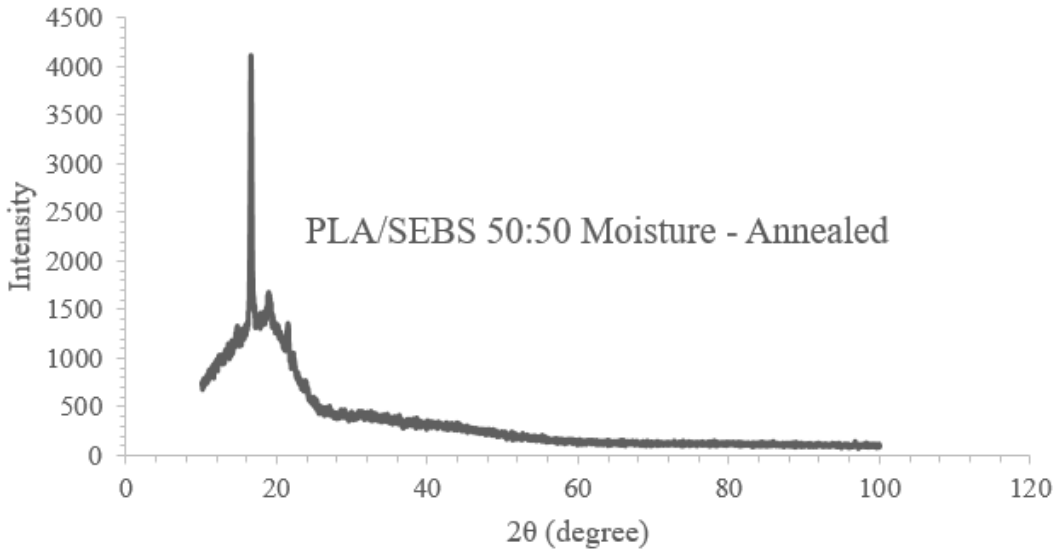

Figure 4.53 XRD spectra for the PLA-SEBS 50/50 – Moisture Annealed Specimen.

CHAPTER 5: SUMMARY AND CONCLUSIONS

The purpose of this work was to explore the effect of an environmental condition on the shape memory properties of a shape memory polymer blend. Specimens fabricated from a shape memory polymer blend composed of polylactic acid (PLA) and styrene ethylene butylene styrene (SEBS) in a 50/50 by weight ratio was subjected to moisture exposure at a temperature of 60 °C for a duration of seven days. The effect on yield strength and shape memory properties, namely the shape fixation and shape recovery ratio were assessed by comparing these parameters to control specimens. In order to determine the effect of the manufacturing process, two fabrication methods were used: 1) injection molding; and 2) the additive manufacturing process of fused filament fabrication.

The main research questions this work sought to answer were: 1) Can environmental degradation be mitigated by heat-induced self-healing mechanisms? 2) What physical or chemical changes are induced by exposure to harsh environments? and 3) Are printed specimens more or less susceptible to environmental degradation?

The experiments carried out in this work consisted of 12 individual sample pools **(**where 8 groups were additively manufactured specimens and 4 were made up of injection molded specimens). Both major groups were internally divided between “Baseline” & “Moisture” specimens for mechanical comparison. All of the 3D printed groups involved the following tensile tests: pulled to failure, pulled to 100% then recovered with heat and then pulled to failure & annealed and then pulled to failure. For the mold injected groups only tensile tests involving pulled to failure & pulled to 100% then recovered with heat and then pulled to failure were done.

This resulted in 48 experimental variants (all in vertical tensile direction): 30 were 3D printed and 18 were fabricated by injection molding. The resulting mechanical properties (tensile

strength, % elongation, and shape memory properties) as well as stress–strain curves were examined after tensile testing to compare all samples. SEM microanalysis was performed to representative specimens from each group in order to determine the fracture behavior. One experimental set involved annealing and analysis by way of X-Ray diffraction was carried out to determine the presence of crystallinity. In every case, exposure to moisture led to a decrease in ultimate tensile strength (UTS) as compared to baseline specimens, though the difference was not statistically significant. The exception to this was specimens that were annealed, which exhibited a decrease in UTS that was statically significantly lower than baseline specimens.

In terms of shape memory properties, exposure to moisture at an elevated temperature did not lead to a statistically significant difference in either the shape recovery ratio (Rr) or shape fixation ratio (Rf) for either injection molded or 3D-printed specimens. It is noted here that 3D printed specimens exhibited superior shape memory property values as compared to injection molded specimens, but the finding is somewhat convoluted due to the fact that shrinkage was observed for the 3D printed specimens when they were recovered. Specimens that were subjected to thermal annealing (based on the known annealing temperature of PLA) experienced severe shrinkage. Though the UTS values were greater than non-annealed specimens, the compromise of specimen geometry along with the afore-mentioned increase in susceptibility to moisture damage makes annealing components fabricated form a 50/50 PLA/SEBS blend ill-advised.

In closing, moisture exposure at elevated temperatures has neither a positive nor a negative effect on the shape memory properties of the polymer blend studied here. This finding is beneficial because it lets a component designer know that this particular material could function in an application that requires shape memory in high humidity, high temperature settings. This work

proves that the shape memory polymer system composed of PLA and SEBS in a 50/50 by weight percent ratio is a shape memory material that can function in a harsh environment.

FUTURE WORKS

There are some ideas that I would have liked to try during the description and the development of the control and recovery of information in Chapter 4. This thesis has been mainly focused on the comparison between additive manufacturing methods and their exposure to environmental degradation, and most of the shape memory properties of the polymers used to find the best results were obtained from the literature or adapted from previous research, leaving the control metrics and numerical variations outside the scope of the thesis along with possible new environmental testing. The following ideas could be tested:

1. Humidity absorption needs to be measured and compared to the sample size by ratio (grams per cm^2). This needs to be done in order to have a proper percentage reference in case bigger specimens and/or different testing materials are used.
2. XRD comparison between injection molded specimens and 3D-printed samples needs to be done along with a baseline/moisture comparison to determine if crystallinity peaks may vary due to environmental exposure factors, material size and/or material type & explain, if possible, why is this happening.
3. Moisture exposure can be done in different processes. Steam chambers can be used to submit samples to water exposure and at the same time observe a possible crystallization due to high temperatures (this written as an assumption).

REFERENCES

Akhbarizadeh, R., Moore, F., & Keshavarzi, B. (2019, April 29). Investigating microplastics bioaccumulation and biomagnification in seafood from the Persian Gulf: a threat to human health? *Food Additives & Contaminants: Part A, 36*(11), 1696-1708.

Andreas Lendlein, M. B. (2010). Shape-memory polymers as technology platform for biomedical applications. *Expert Review of Medical Devices*, 357-379.

Andreas Lendlein, O. E. (2019). Reprogrammable recovery and actuation behaviour of shape-memory polymers. *Nature Reviews Materials*, 116–133.

Aschberger, K., Castello, P., Hoekstra, E., Karakitsios, S., & S. Munn, S. (2010). Bisphenol A and baby bottles: challenges. *JRC Scientific and Technical Reports*, 1-57.

Bergmann, M., Collard, F., Fabres, J., Gabrielsen, G. W., Provencher, J. F., Rochman, C. M., . . . Tekman, M. B. (2022, April 05). Plastic pollution in the Arctic. *Nature Reviews Earth & Environment, 3*, 323–337.

Chávez, F. A., Siqueiros, J. G., Carrete, I. A., Delgado, I. L., Ritter, G. W., & Roberson, D. A. (2019). Characterisation of phases and deformation temperature for additively manufactured shape memory polymer components fabricated from rubberised acrylonitrile butadiene styrene. *Virtual and Physical Prototyping*, 188-202.

Chen, X., Xu, S., Tan, T., Lee, S. T., Cheng, S. H., Lee, F. W., . . . Ho, K. C. (2014, March). Toxicity and Estrogenic Endocrine Disrupting Activity of Phthalates and Their Mixtures. *International Journal of Environmental Research and Public Health, 1*(3), 3156-3168.

Cox, K. D., Covernton, G. A., Davies, H. L., Dower, J. F., Juanes, F., & Dudas, S. E. (2019, June 05). Human Consumption of Microplastics. *Environmental Science & Technology, 53*(12), 7068–7074.

Cussler, E. L. (2009). Diffusion: Mass Transfer in Fluid Systems. *Cambridge Univ. Press*.

Diego Bermudez; Paulina A. Quinonez; Evelin J. Vasquez; Israel A. Carrete; Truman J. Word & David A. Roberson. (2021). A comparison of the physical properties of two commercial 3D printing PLA grades. *Virtual and Physical Prototyping, 16*(2), 178-195.

Dizon, J. R., Jr., A. H., Chen, Q., & Advincula, R. C. (2018, March). Mechanical characterization of 3D-printed polymers. *Additive Manufacturing*(20), 44-67.

Dong, G. M. (2022). Effect of amplitude ratios on hole quality in longitudinal–torsional coupled ultrasonic-assisted drilling of CFRP composites. *The International Journal of Advanced Manufacturing Technology*.

Egger, M., Sulu-Gambari, F., & Lebreton, L. (2020, May 06). First evidence of plastic fallout from the North Pacific Garbage Patch. *Scientific Reports, 10*, 7495.

Ema, M., Fujii, S., Furukawa, M., Kiguchi, M., Ikka, T., & Harazono, A. (2001, September-October). Rat two-generation reproductive toxicity study of bisphenol A. *Reproductive Toxicology, 15*(5), 505-523.

Eriksen, M., Maximenko, N., Thiel, M., Cummins, A., Lattin, G., Wilson, S., . . . Rifman, S. (2013, March). Plastic pollution in the South Pacific subtropical gyre. *Marine Pollution Bulletin, 68*(1-2), 71-76.

Garces, I. T., & Ayranci, C. (2021, January 27). Advances in additive manufacturing of shape memory polymer composites. *27*(2), 1355-2546.

Gongora, J. P. (Septiembre y Octubre de 2014). La industria del plastico en Mexico y el mundo. *Comercio Exterior, 64*(5), 1-2.

Guzzetti, E., Sureda, A., SilviaTejada, & Faggio, C. (2018, December). Microplastic in marine organism: Environmental and toxicological effects. *Environmental Toxicology and Pharmacology, 64*, 164-171.

Hager, M. D., Bode, S., ChristineWeber, & Schubert, U. S. (2015, October-November). Shape memory polymers: Past, present and future developments. *Progress in Polymer Science, 49-50*, 3-33.

Hamidian, K. Z., Tubić, A., Zhang, Y., Fang, J. K., Wu, C., & Lam, P. K. (2021, April 1). Understanding plastic degradation and microplastic formation in the environment: A review. *Environmental Pollution, 274*, 116554.

Hermabessiere, L., Dehaut, A., Paul-Pont, I., CamilleLacroix, Jezequel, R., Soudant, P., & Duflos, G. (2017, September). Occurrence and effects of plastic additives on marine environments and organisms: A review. *Chemosphere, 182*, 781-793.

Horn, D. A., Granek, E. F., & Steele, C. L. (2019, December 30). Effects of environmentally relevant concentrations of microplastic fibers on Pacific mole crab (Emerita analoga) mortality and reproduction. *Limnology and Oceanography Letters*, 74-83.

Kim, E., Shin, Y.-J., & Ahn, S.-H. (2016, October 17). The effects of moisture and temperature on the mechanical properties of additive manufacturing components: fused deposition modeling. *Rapid Prototyping Journal, 22*(6), 887-894.

Komal, U. K., Kasaudhan, B. K., & Singh, I. (2021, May 20). Comparative Performance Analysis of Polylactic Acid Parts Fabricated by 3D Printing and Injection Molding. *Journal of Materials Engineering and Performance volume, 30*, 6522–6528.

KosukeTanaka, HideshigeTakada, ReiYamashita, Mizukawa, K., Fukuwaka, M.-a., & Watanuki, Y. (2013, April 15). Accumulation of plastic-derived chemicals in tissues of seabirds ingesting marine plastics. *Marine Pollution Bulletin, 69*(1-2), 219-222.

Kristen, U., Sheela, S., De, R. A., M., K. H., Delia, S., & L., H. V. (2014, November). A population-based case–control study of urinary bisphenol A concentrations and risk of endometriosis. *Human Reproduction, 29*(11), 2457–2464.

Kühn, S., Schaafsma, F. L., Werven, B. v., Flores, H., Bergmann, M., Egelkraut-Holtus, M., . . . Franeker, J. A. (2018, February 20). Plastic ingestion by juvenile polar cod (Boreogadus saida) in the Arctic Ocean. *Polar Biology, 41*, 1269–1278.

Kumar, K. S., Biju, R., & Nair, C. R. (2013, February). Progress in shape memory epoxy resins. *Reactive and Functional Polymers, 73*(2), 421-430.

Lantada, A. D. (2017, September 29). Systematic Development Strategy for Smart Devices Based on Shape-Memory Polymers. *Polymers, 9*(10), 496.

Lei, M., Chen, Z., Lu, H., & Yu, K. (2019, December 04). Recent progress in shape memory polymer composites: methods, properties, applications and prospects. *Nanotechnology Reviews, 8*(5), 1-25.

Lendlein, A., & Kelch, S. (2002, June 17). Shape-Memory Polymers. *Angewandte Chemie, 41*(12), 2034-2057.

Li Sun, W. M. (2010). Mechanisms of the multi-shape memory effect and temperature memory effect in shape memorypolymers. *Royal Society of Chemistry*, 4403-4406.

Liu, G., Ding, X., Cao, Y., Zheng, Z., & Peng, Y. (2005, April 22). Novel Shape-Memory Polymer with Two Transition Temperatures. *Macro Molecular Rapid Communications, 26*(8), 649-652.

Liu, Y., Gall, K., Dunn, M. L., & McCluskey, P. (2003, November 20). Thermomechanical recovery couplings of shape memory polymers in flexure. *Smart Materials and Structures, 12*(6), 947.

Mohadeseh Zare, M. P. (2019). Thermally-induced two-way shape memory polymers: Mechanisms, structures, and applications. *Chemical Engineering Journal*, 706-720.

Mohr, R. e. (2006). Initiation of shape-memory effect by inductive heating of magnetic nanoparticles in thermoplastic polymers. *Proc. Natl Acad. Sci. USA*, 3540–3545.

Monteiro, R. C., Sul, J. A., & F.Costa, M. (2018, July). Plastic pollution in islands of the Atlantic Ocean. *Environmental Pollution, 238*, 103-110.

Narayan, R. (2017, February 16). Biodegradable and Biobased Plastics: An Overview. *Soil Degradable Bioplastics for a Sustainable Modern Agriculture*, 23–34.

P.Butaud, Placet, V., Klesa, J., Ouisse, M., Foltête, E., & Gabrion, X. (2015, August). Investigations on the frequency and temperature effects on mechanical properties of a shape memory polymer (Veriflex). *Mechanics of Materials, 87*, 50-60.

Paulina A. Quinonez, L. U.-S.-W. (2021). Design of Shape Memory Thermoplastic Material Systems for FDM-Type Additive Manufacturing. *Materials*, 1-19.

Pavia, U. D. (2022, 08 25). *COMPMECH*. Retrieved from Computational Mehcanics & Advanced Materials: https://compmech.unipv.it/research-activities/advanced-materials/constitutive-modeling-of-shape-memory-polymers/

Pilate, F., Toncheva, A., Dubois, P., & Raquez, J.-M. (2016, June). Shape-memory polymers for multiple applications in the materials world. *European Polymer Journal, 80*, 268-294.

Qi, H. J., Nguyen, T. D., Castro, F., Yakacki, C. M., & Shandas, R. (2008, May). Finite deformation thermo-mechanical behavior of thermally induced shape memory polymers. *Journal of the Mechanics and Physics of Solids, 56*(5), 1730-1751.

Rainer, W. C.-s. (1964). *US Patent No. 3144398.*

Sakai, S.-i., Yoshida, H., Hirai, Y., Asari, M., Takigami, H., Takahashi, S., . . . Fischer, C. (2011, May 18). International comparative study of 3R and waste management policy developments. *Journal of Material Cycles and Waste Management, 13*, 86-102.

Schwabl, P., Köppel, S., Dipl-Ing, Königshofer, P., Bucsics, T., Trauner, M., . . . Liebmann, B. (2019, October 01). Detection of Various Microplastics in Human Stool. *Annals of Internal Medicine*, 1-6.

Sharma, S., & Chatterjee, S. (2017, September 16). Microplastic pollution, a threat to marine ecosystem and human health: a short review. *Environmental Science and Pollution Research, 24*, 21530–21547.

Sherri L. Messimer, T. R. (2019). Full-Density Fused Deposition Modeling Dimensional Error as a Function of Raster Angle and Build Orientation: Large Dataset for Eleven Materials. *Journal of Manufacturing and Materials Processing* , 27.

Shi, Y., Yoonessi, M., & Weiss, R. A. (2013, May 02). High Temperature Shape Memory Polymers. *Macromolecules, 46*(10), 4160–4167.

Siqueiros, J. Gilberto; Schnittker, Kevin & Roberson, David A. (2016). ABS-maleated SEBS blend as a 3D printable material. *Virtual and Physical Prototyping, 11*(2), 123-131.

Slat, B. (2022, 08 25). *The Ocean Cleanup*. Retrieved from The Ocean Cleanup: https://theoceancleanup.com/great-pacific-garbage-patch/

Smith, M., Love, D. C., Rochman, C. M., & Neff, R. A. (2018, August 16). Microplastics in Seafood and the Implications for Human Health. *Food, Health, and the Environment, 5*, 375–386.

Sokolowski, W., Metcalfe, A., Hayashi, S., Yahia, L., & Raymond, J. (2007, March 02). Medical applications of shape memory polymers. *Biomedical Materials, 2*(1), S23.

Sokolowski, W., Metcalfe, A., Hayashi, S., Yahia, L., & Raymond2, J. (2007, March 02). Medical applications of shape memory polymers. *Biomedical Materials, 2*(1), S23.

Suaria, G., Perold, V., Leed, J. R., Lebouard, F., Aliani, S., & G.Ryan, P. (2020, March). Floating macro- and microplastics around the Southern Ocean: Results from the Antarctic Circumnavigation Expedition. *Environment International, 136*, 105494.

Sul, J. A., & Costa, M. F. (2007, August). Marine debris review for Latin America and the Wider Caribbean Region: From the 1970s until now, and where do we go from here? *Marine Pollution Bulletin, 54*(8), 1087-1104.

TaoXu, GuoqiangLi, & Pang, S.-S. (2011, October). Effects of ultraviolet radiation on morphology and thermo-mechanical properties of shape memory polymer based syntactic foam. *Composites Part A: Applied Science and Manufacturing, 42*(10), 1525-1533.

Turner, A., & Filella, M. (2021, November). Hazardous metal additives in plastics and their environmental impacts. *Environment International, 156*, 106622.

Vernon, L. B. (1941). *US Patent No. 2234993.*

Welle, F., & Franz, R. (2018, August 26). Microplastic in bottled natural mineral water – literature review and considerations on exposure and risk assessment. *Food Additives and Contaminants: Part A, 35*(12), 2482-2492.

Westbrook, K. K., Kao, P. H., Castro, F., Ding, Y., & Qi, H. J. (2011, December). A 3D finite deformation constitutive model for amorphous shape memory polymers: A multi-branch modeling approach for nonequilibrium relaxation processes. *Mechanics of Materials, 43*(12), 853-869.

Wicks, F. (2007, June). Plastic arts: the chemistry that has formed so many of the objects in our world traces its roots to an accidental discovery 100 years ago. *Mechanical Engineering-CIME, 129*(6), 44+.

Xia, Y., He, Y., Zhang, F., Liu, Y., & Leng, J. (2020, September 23). A Review of Shape Memory Polymers and Composites: Mechanisms, Materials, and Applications. *Advanced Materials, 33*(6), 1-33.

Yakacki, C., S. Willis, C. L., & Gall, K. (2008, February 12). Deformation Limits in Shape-Memory Polymers. *Advanced Engineering Materials, 10*(1-2), 112-119.

Zarek, M., Layani, M., Cooperstein, I., Sachyani, E., Cohn, D., & Magdassi, S. (2015, September 24). 3D Printing of Shape Memory Polymers for Flexible Electronic Devices. *Advanced Materials, 28*(22), 4449-4454.

Ziccardi, L. M., Edgington, A., Hentz, K., Kulacki, K. J., & Driscoll, S. K. (2016, April 16). Microplastics as vectors for bioaccumulation of hydrophobic organic chemicals in the marine environment: A state-of-the-science review. *Environmental Toxicology and Chemistry, 35*(7), 1667-1676.

GLOSSARY

Term	Definition
SMP	Shape Memory Polymer (Belongs to the class of smart materials and are defined as those polymers that have the ability to return from a deformed state (temporary shape) to that original (permanent form) through an external stimulus.)
PLA	Polylactic Acid (Is a type of plastic that is used in building models and prototypes of solid objects and components. It is a thermoplastic polyester that serves as the raw material in 3-D printing or additive manufacturing processes and applications.)
SEBS	Styrene-ethylene-butylene-styrene (Is an important thermoplastic elastomer (TPE) which behaves like rubber without undergoing vulcanization. Is strong and flexible, has excellent heat and UV resistance and is easy to process.)
ASTM	American Society for Testing and Materials (Is a developer of international voluntary consensus standards. ASTM standards are developed by committees of relevant industry professionals who meet regularly in an open and transparent process to deliver standards, test methods, specifications, guides, and practices.)
SEM	Scanning Electron Microscopy (Is formed by a beam of electrons focused to a few billionths of a meter that is swept across the surface of a sample in a series of stacked rows until a complete two-dimensional pattern is formed. As the beam strikes solid electrons are emitted from the specimen and those particles are collected to form an image.)
XRD	X-ray diffraction analysis (Is a technique used in materials science to determine the crystallographic structure of a material. XRD works by irradiating a material with incident X-rays and then measuring the intensities and scattering angles of the X-rays that leave the material.)

VITA

Jorge Avila was born and raised in Ciudad Juarez, Chihuahua, Mexico. Before attending The University of Texas at El Paso (UTEP) for his master's studies in Metallurgical and Materials Engineering, he attended to Instituto Tecnologíco y de Estudios Superiores de Monterrey (ITESM), Campus Juarez, where he earned a Bachelor of Mechatronic Engineering, with a general grade average of 90.29, in 2017. From 2013 to 2016, he also attended to Centro de Entrenamiento en Alta Tecnología (CENALTEC), Campus Juarez, where he received an official Technical Certificate in Plastic Injection Molding.

While at ITESM, Jorge participated on different workshops including CMC Machine Tooling (Milling and Turnstile) and Circuit Design with PCB Manufacturing. He also got awarded with the first place on Jornadas Mecatronicas 2013 (Mechatronic Days) and second place on Jornadas Mecatronicas 2015 for his Lunar Bot and Automated Greenhouse projects respectively.

Since graduating from Bachelor's, Jorge has been working for different enterprises, from 2017 to 2021 he worked at Robert Bosch JuP1 (Juarez, Mx.) as a Product Coordinator Intern (2017-2018) and as a Process Engineer (2018-2021). From 2021-2022, he worked as an MRO Technical Services Engineer at SDI Distribution at client site (ECI J1 & J2 in Juarez, Mx.) mainly focusing on engineering counsellorship.

Currently, Jorge has been accepted for the PhD in Materials and Advance Science & Engineering program at The University of Texas at El Paso starting full-time this Spring 2023 and has been awarded with a CONACYT scholarship with full paid tuition for his PhD studies. He lives in Ciudad Juarez, Chihuahua, Mexico.

Contact Information: jorgemario094@gmail.com